Paleoseismology of Utah, Volume 18

PALEOSEISMIC INVESTIGATION OF THE NORTHERN WEBER SEGMENT OF THE WASATCH FAULT ZONE AT THE RICE CREEK TRENCH SITE, NORTH OGDEN, UTAH

by Christopher B. DuRoss, Stephen F. Personius, Anthony J. Crone, Greg N. McDonald, and David J. Lidke

SPECIAL STUDY 130
UTAH GEOLOGICAL SURVEY
a division of
UTAH DEPARTMENT OF NATURAL RESOURCES
2009

Utah Geological Survey
60 years
1949 2009
Excellence, Integrity, and Objectivity

Paleoseismology of Utah, Volume 18

PALEOSEISMIC INVESTIGATION OF THE NORTHERN WEBER SEGMENT OF THE WASATCH FAULT ZONE AT THE RICE CREEK TRENCH SITE, NORTH OGDEN, UTAH

by Christopher B. DuRoss[1], Stephen F. Personius[2], Anthony J. Crone[2], Greg N. McDonald[1], and David J. Lidke[2]

[1]Utah Geological Survey
[2]U.S. Geological Survey

Cover photo: *Rice Creek trench site; view is to the east.*

ISBN 1-55791-819-8

SPECIAL STUDY 130
UTAH GEOLOGICAL SURVEY
a division of
UTAH DEPARTMENT OF NATURAL RESOURCES
2009

STATE OF UTAH
Gary R. Herbert, Governor

DEPARTMENT OF NATURAL RESOURCES
Michael Styler, Executive Director

UTAH GEOLOGICAL SURVEY
Richard G. Allis, Director

PUBLICATIONS
contact
Natural Resources Map & Bookstore
1594 W. North Temple
Salt Lake City, UT 84116
telephone: 801-537-3320
toll-free: 1-888-UTAH MAP
Web site: mapstore.utah.gov
email: geostore@utah.gov

UTAH GEOLOGICAL SURVEY
contact
1594 W. North Temple, Suite 3110
Salt Lake City, UT 84116
telephone: 801-537-3300
Web site: geology.utah.gov

Although this product represents the work of professional scientists, the Utah Department of Natural Resources, Utah Geological Survey, makes no warranty, expressed or implied, regarding its suitability for a particular use. The Utah Department of Natural Resources, Utah Geological Survey, shall not be liable under any circumstances for any direct, indirect, special, incidental, or consequential damages with respect to claims by users of this product.

CONTENTS

FOREWORD ix
ABSTRACT 1
INTRODUCTION 1
Geologic Setting 2
Wasatch Fault Zone 2
Weber Segment 2
Previous Investigations 2
Why Trench the Weber Segment? 2
RICE CREEK SITE 5
Geologic Setting 5
Surface Offset 7
Trench Excavations 8
Radiocarbon Dating 9
Sampling and Dating Strategy 9
Sources of Dating Uncertainty 11
Luminescence Dating 11
OxCal Modeling 12
RICE CREEK TRENCH INVESTIGATION 12
Stratigraphy 12
Alluvial-Fan Deposits 12
Scarp-Derived Colluvium 12
Fault-Zone Geometry 13
Surface Faulting at the Rice Creek Site 13
Upper Fault Zone 13
Earthquake U3 13
Earthquake U2 14
Earthquake U1 15
Earthquake AU1 15
Per-event displacement 15
Lower Fault Zone 16
Earthquakes L4 and L3 16
Earthquake L2 16
Earthquake L1 17
Earthquakes AL2 and AL1 17
Per-event displacement 17
Correlation of Earthquakes 18
RICE CREEK EARTHQUAKE PARAMETERS 18
Earthquake Timing and Displacement 18
Earthquake Recurrence and Vertical Slip Rate 20
DISCUSSION OF RESULTS 23
CONCLUSIONS 25
ACKNOWLEDGMENTS 25
REFERENCES 26
APPENDICES 29
APPENDIX A. Description of Stratigraphic Units 30
APPENDIX B. Summary of ^{14}C-dated charcoal 33
APPENDIX C. Quartz blue-light optically stimulated luminescence ages 34
APPENDIX D. OxCal models 35
APPENDIX E. Slip-rate estimates for the Rice Creek site 37

FIGURES

Figure 1. Physiographic provinces of Utah and surrounding states....3
Figure 2. Surface trace of the Brigham City, Weber, and Salt Lake City segments of the Wasatch fault zone....4
Figure 3. Northern Weber segment....6
Figure 4. Surficial geologic map of the Rice Creek site....7
Figure 5. Topographic map of the Rice Creek site....8
Figure 6. Scarp-profile and surface-slope information for the Rice Creek site....9
Figure 7. Photographs of the Rice Creek site....10
Figure 8. Sampling strategy for the Rice Creek site....14
Figure 9. Earthquake time ranges....19
Figure 10. Stratigraphic ordering and numerical control for the Rice Creek site....22
Figure 11. Comparison of earthquake-timing data for the Weber segment....24

TABLES

Table 1. Summary of existing earthquake timing data for the Weber segment....5
Table 2. Per-event vertical displacement estimates for the Rice Creek site....16
Table 3. Correlation of earthquakes at the Rice Creek site....20
Table 4. OxCal output for model D....21
Table 5. Summary of earthquake parameters for the Rice Creek site....23

PLATES

Plate 1. Stratigraphic and structural relations at the Rice Creek site....on CD
Plate 2. Structural restoration of the main trench, Rice Creek site....on CD

FOREWORD

This Utah Geological Survey Special Study, *Paleoseismic Investigation of the Northern Weber Segment of the Wasatch Fault Zone at the Rice Creek Trench Site, North Ogden, Utah,* is the eighteenth report in the Paleoseismology of Utah series. This series makes the results of paleoseismic investigations in Utah available to geoscientists, engineers, planners, public officials, and the general public. These studies provide critical information regarding paleoearthquake parameters such as earthquake timing, recurrence, displacement, slip rate, fault geometry, and segmentation, which can be used to characterize potential seismic sources and evaluate the long-term seismic hazard of Utah's Quaternary faults.

This report presents new paleoseismic information for the northern Weber segment of the Wasatch fault zone, collected as part of a joint Utah Geological Survey and U.S. Geological Survey seismic-hazard evaluation. The purpose of the study was to address uncertainties in the number, timing, and displacement of surface-faulting earthquakes on the segment. To address these issues, two trenches were excavated at Rice Creek in North Ogden. The trenches exposed evidence for three surface-faulting earthquakes in an upper fault zone, four earthquakes in a lower fault zone, and two earthquakes in an antithetic fault zone. Using stratigraphic and structural relations, and radiocarbon and luminescence ages, the earthquakes within the three fault zones were resolved into a preferred scenario of six Holocene earthquakes at the site. The study also substantiated an approximately 500-year-old earthquake identified in a previous investigation on the northern Weber segment that may represent a partial-segment rupture.

Determining well-constrained paleoseismic parameters for the Weber segment is important because the new data will help refine fault segmentation and hazard models and improve earthquake-hazard evaluations for the region, all of which help reduce Utah's earthquake-related risk.

William R. Lund, Editor
Paleoseismology of Utah Series

PALEOSEISMIC INVESTIGATION OF THE NORTHERN WEBER SEGMENT OF THE WASATCH FAULT ZONE AT THE RICE CREEK TRENCH SITE, NORTH OGDEN, UTAH

by Christopher B. DuRoss, Stephen F. Personius, Anthony J. Crone, Greg N. McDonald, and David J. Lidke

ABSTRACT

This report contains new paleoseismic information for the Weber segment of the Wasatch fault zone (WFZ), collected as part of a joint Utah Geological Survey and U.S. Geological Survey seismic-hazard evaluation. We excavated two fault trenches at the Rice Creek site in the spring of 2007 to address uncertainties in the number, timing, and displacement of surface-faulting earthquakes on the segment. Our new data better define the Holocene surface-faulting activity of the northern Weber segment by (1) refining estimates of paleoearthquake timing, displacement, recurrence, and vertical slip rate; (2) providing timing information for a previously unknown sixth earthquake in the early Holocene; and (3) substantiating the ~500-yr earthquake found in a previous investigation 9 km to the south. These results are important for understanding segmentation of the northern WFZ and for improving earthquake-hazard evaluations of the region.

We excavated two trenches across two 8- and 4-m-offset, down-to-the-west scarps and a 1-m-offset antithetic scarp, and found evidence for three surface-faulting earthquakes in an upper fault zone, four earthquakes in a lower fault zone, and two earthquakes in an antithetic fault zone. Using stratigraphic and structural relations, radiocarbon and luminescence ages, and the results of OxCal modeling, we developed a preferred scenario of six Holocene earthquakes at the site. Earthquake 6 occurred before 7810–9930 yr, during a period of active alluvial-fan deposition, and had a minimum of 0.6–0.7 m of vertical displacement. Earthquake 5 faulted the ground surface 1.6–2.3 m at 5500–7530 cal yr B.P., and in our preferred scenario, earthquakes 4 and 3 occurred separately at 3690–5370 cal yr B.P. and 1790–3670 cal yr B.P., with 1.6–2.3 m and 0.8–1.4 m of displacement, respectively. However, poor timing information for earthquake 3 creates uncertainty regarding the interpretation of earthquakes 4 and 3 as separate events. Strong stratigraphic and chronological evidence shows that the youngest earthquakes occurred at 750–1350 cal yr B.P. (earthquake 2) and 490–630 cal yr B.P. (earthquake 1), with 2.7–3.7 m and 1.3–2.7 m of displacement, respectively.

Fault and earthquake parameters for the site are based on our preferred six-earthquake scenario. Our preferred total site displacement is 8.0–12.4 m, which reflects the per-event displacements of all post-fan earthquakes and encompasses net-displacement estimates based on the projection of geomorphic surfaces (8.5–11.4 m), graphical reconstruction of faulting (9.5–9.9 m), and scarp-profile data (net surface offset of 9.3–11.5 m). Per-event displacements range from 0.6 to 3.7 m and average 1.6–2.5 m for earthquakes 5 to 1. The mean Holocene recurrence interval between earthquakes 5 and 1 is 1500 yr, with an estimated two-sigma range of 500–3100 yr. Holocene vertical slip rates range from 0.8 to 3.0 mm/yr and average 0.9–2.1 mm/yr, which is our preferred estimate based on net site displacement and surface offset, elapsed time between the youngest and oldest earthquakes, and age of the fan sediments.

INTRODUCTION

Fault trenches excavated in the spring of 2007 at the Rice Creek site by the Utah Geological Survey (UGS) and U.S. Geological Survey (USGS) provide new paleoseismic data for the northern Weber segment of the Wasatch fault zone (WFZ). The Rice Creek data extend the record of large-magnitude surface-faulting earthquakes on the segment into the early Holocene, and refine fault and earthquake parameters including earthquake timing, displacement, recurrence, and vertical slip rate. These data are essential to (1) improve the correlation of earthquakes among trench sites on the Weber segment, (2) infer earthquake rupture length and magnitude, and (3)

compare the Weber segment paleoseismic record with those for the adjacent Brigham City and Salt Lake City segments. These data will help reduce losses from future earthquakes in Utah by improving the characterization of earthquake sources for probabilistic earthquake-hazard analyses of the Wasatch Front region (e.g., the National Seismic Hazard Maps; USGS, 2008).

Geologic Setting

Wasatch Fault Zone

The 343-km-long WFZ extends along the western base of the Wasatch Range, forming the boundary between the Basin and Range and Middle Rocky Mountain physiographic provinces in north-central Utah (figure 1a). The WFZ presents a significant earthquake hazard to Utah's heavily urbanized Wasatch Front and its earthquake history is important in understanding the spatial and temporal trends of surface-faulting earthquakes in the Basin and Range Province. The WFZ accommodates east-west extension at the eastern edge of the Basin and Range Province (Martinez and others, 1998; Chang and others, 2006) (figure 1a), and releases strain in large-magnitude (M 6.7–7.3) surface-faulting earthquakes along quasi-independent seismogenic fault segments (Swan and others, 1980; Schwartz and Coppersmith, 1984). Ten segments have been delineated based on structural, geological, geophysical, and seismological data (Machette and others, 1992). Variations in the fault's Holocene rupture history and the geometry of late Quaternary fault traces are the primary evidence for the central six segments from near Brigham City to Levan (figure 1b; Swan and others, 1980; Schwartz and Coppersmith, 1984; Machette and others, 1992; Lund, 2005). Recent advances in understanding the earthquake history of the central WFZ include refinements of latest Pleistocene paleoseismic records (McCalpin, 2002; McCalpin and Forman, 2002; Olig and others, 2004) and evaluations of the potential for partial- and multiple-segment ruptures on the fault (e.g., Chang and Smith, 2002; DuRoss, 2008).

The five central segments of the WFZ from Brigham City to Nephi each have evidence for multiple surface-faulting earthquakes in the past 6000 yr. During the Holocene, surface faulting has recurred approximately every 1300–2500 yr on individual segments (Lund, 2005), and averaged every 350–400 yr for the five segments collectively (Machette and others, 1992; McCalpin and Nishenko, 1996). The segments are 36–59 km long (straight-line distance; Machette and others, 1992; Black and others, 2003), have a mean vertical displacement of 2.2 ± 1.0 m (one sigma) per surface-faulting earthquake (DuRoss, 2008), and mean Holocene vertical slip rates of about 1.1–1.4 mm/yr (Lund, 2005). The contemporary rate of horizontal extension across the central WFZ is 1.6 ± 0.4 mm/yr, based on campaign (1992–2003) and continuous (1997–2004) GPS data, assuming spatially homogeneous strain in a 65-km-wide zone extending along the WFZ from near Brigham City to Nephi (Chang and others, 2006).

Weber Segment

The Weber segment presents a significant earthquake hazard to the Wasatch Front between Salt Lake City and Brigham City (figure 2). The segment is the second longest WFZ segment, having a 56-km-long surface-trace length that is mostly linear, but becomes more complex (e.g., including multiple overlapping fault traces) at both ends (figure 2) (Nelson and Personius, 1993). DuRoss (2008) calculated a mean (n=10) vertical displacement of 2.1 ± 1.3 m (one sigma) for individual Weber-segment earthquakes. Based on empirical fault length and per-event displacement–magnitude regressions for normal-faulting earthquakes (Wells and Coppersmith, 1994), the Weber segment is capable of generating earthquakes of moment magnitude 7.0–7.2 (DuRoss, 2008).

Previous Investigations

Information on the timing, displacement, and extent of surface-faulting earthquakes on the Weber segment are from two prior paleoseismic studies (figure 2): one at Kaysville, where Swan and others (1980, 1981) and McCalpin and others (1994) completed trenching studies more than a decade apart, and the other at East Ogden (Nelson, 1988; Forman and others, 1991; Nelson and others, 2006). The study of a cut-slope excavation at Garner Canyon (figure 2) provided additional earthquake information for the northern part of the segment (Machette and others, 1992; Nelson and Personius, 1993; Nelson and others, 2006).

The Kaysville, East Ogden, and Garner Canyon paleoseismic sites each exposed evidence of at least three large-displacement surface-faulting earthquakes during the Holocene (table 1). However, questions remain regarding the correlation of these earthquakes because of large uncertainties in earthquake timing and a possible partial-segment rupture at ~500 yr proposed at the East Ogden site (Nelson and others, 2006). Alternative reconstructions of the Weber segment earthquake chronology depend on different earthquake correlations, and affect earthquake recurrence and vertical-slip-rate estimates for the segment.

Why Trench the Weber Segment?

A complete and consistent record of earthquakes on the WFZ is critical for developing and refining models of surface-faulting earthquake recurrence, displacement, and segmentation, all of which influence earthquake-hazard evaluations for the region. However, the difficulty in correlating individual earthquakes among the previous Weber-segment paleoseismic sites increases uncertainties in earthquake-hazard assessments for this densely urbanized part of the Wasatch Front. The Utah Quaternary Fault Parameters Working Group (UQFPWG; Lund, 2005) concurred that the Weber segment had the least well-understood history of surface-faulting earthquakes of the five central segments of the WFZ and recommended additional trenching to update and improve paleoseismic parameters.

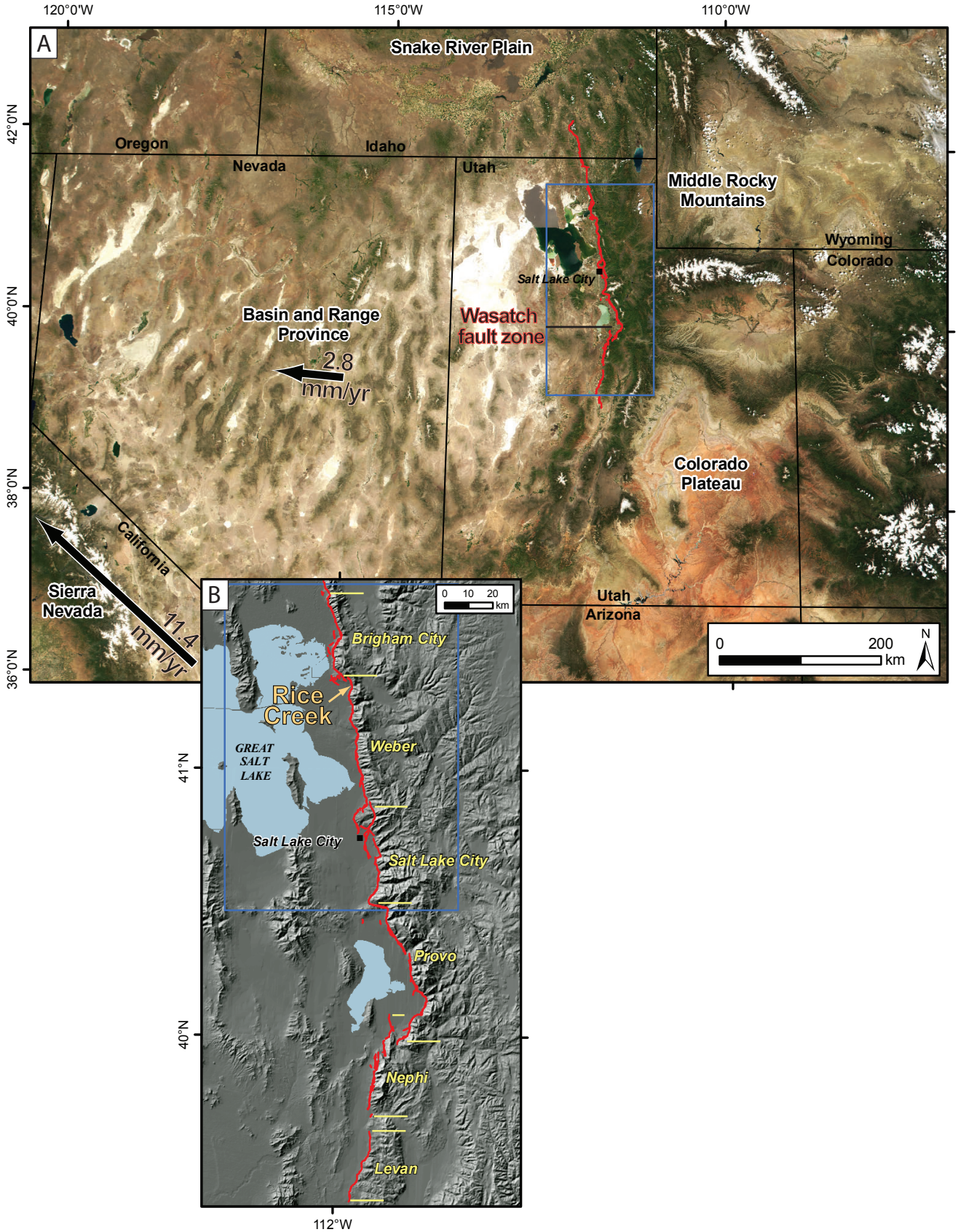

Figure 1. *(A) Physiographic provinces of Utah and surrounding states. Arrows indicate approximate geodetic motion vectors and rates of the central Basin and Range Province and Sierra Nevada areas relative to the Colorado Plateau (modified from Bennett and others, 2003). Box outlined in blue is area of figure 1B. True-color satellite image from National Aeronautics & Space Administration (NASA, 2006), taken May 31, 2001. (B) Central segments of the Wasatch fault zone. Horizontal yellow lines indicate segment boundaries. Box outlined in blue is area of figure 2.*

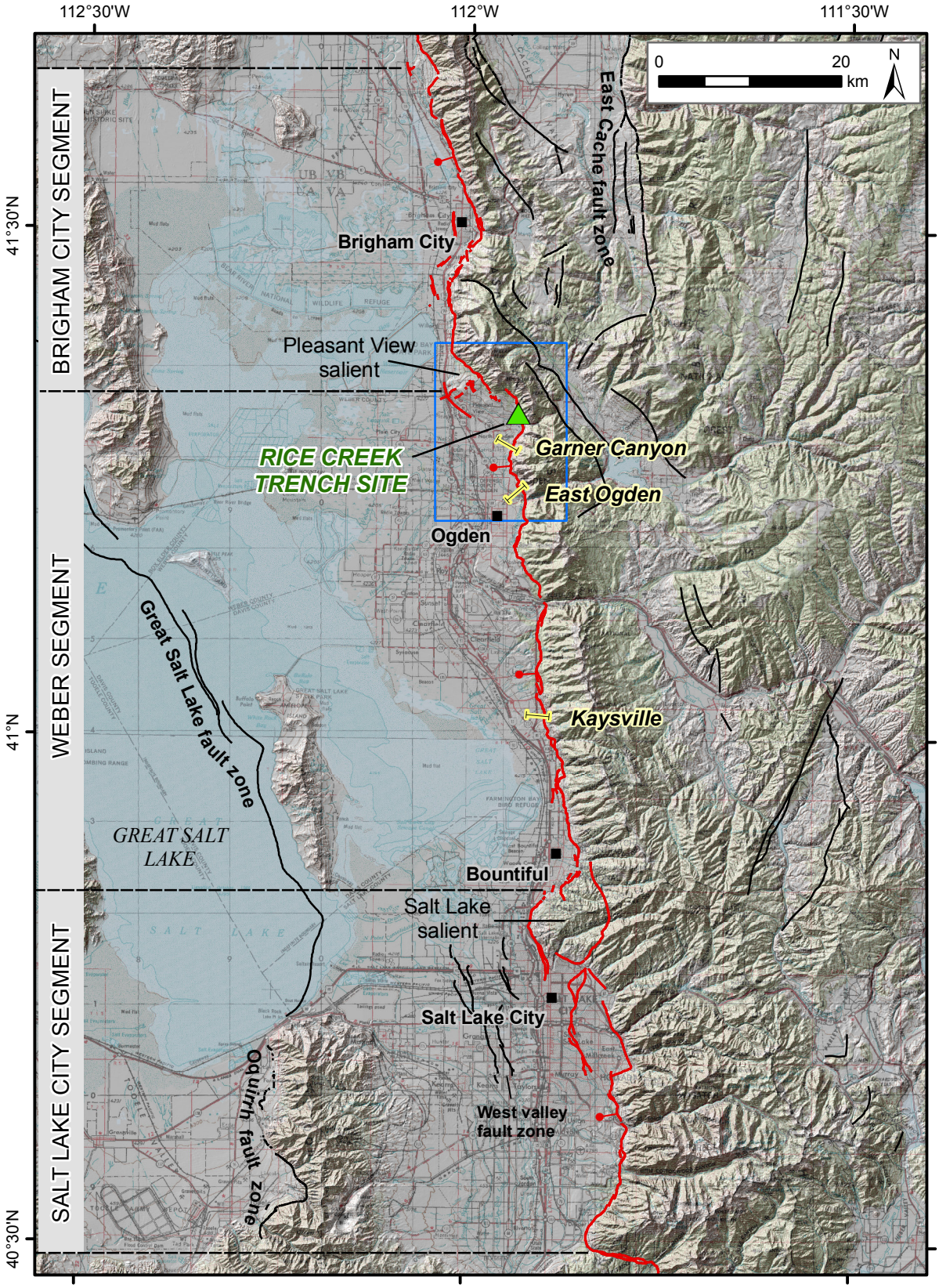

Figure 2. Surface trace of the Brigham City, Weber, and Salt Lake City segments of the Wasatch fault zone (WFZ) showing locations of the Rice Creek site, and pre-2007 paleoseismic sites (I shapes). Trace of WFZ (red) and other Quaternary faults (black) from Black and others (2003); ball and bar on downthrown side. Box outlined in blue is area of figure 3. Basemaps: scanned 1:250,000-scale topographic map and 30-m digital elevation model.

Table 1. *Summary of existing earthquake timing data for the Weber segment.*[1]

Kaysville site (cal yr B.P.)[2]	East Ogden site (cal yr B.P.)[3]	Garner Canyon site (cal yr B.P.)[3]	UQFPWG (cal yr B.P.)[4]
no evidence*	200–600 (D)	no evidence (D)	500 ± 300
600–800 (Z)*	**500–1700 (C)**	**600–1500 (C)**	950 ± 450
2100–3500 (Y)	**2400–3900 (B)**	**1400–2800 (B)**	3000 ± 700
no evidence	2800–4800 (A)	>2100–2800 (A)	4500 ± 700
3800–7900 (5700–6100) (X)	not exposed?	not exposed?	6100 ± 700

[1] Surface-faulting earthquakes identified at existing fault trench sites on the Weber segment. Bold text indicates earthquakes that correlate among all three trench sites, based on Nelson and others (2006).

[2] Earthquake chronology summarized from McCalpin and others (1994). *The original Kaysville trench investigation (Swan and others, 1980, 1981) found evidence for two earthquakes younger than 1200–1800 cal yr B.P. (1580 ± 180 ^{14}C yr B.P.).

[3] Earthquake chronology (and lettering scheme) summarized from Nelson and others (2006).

[4] Consensus preferred earthquake times and uncertainties from the Utah Quaternary Fault Parameters Working Group (Lund, 2005).

The joint UGS–USGS study at Rice Creek sought to (1) improve information on the timing and displacement of surface-faulting earthquakes, which are only broadly constrained from existing studies (table 1), (2) identify the youngest earthquakes on the northern part of the Weber segment, (3) reduce uncertainties in earthquake-recurrence and slip-rate estimates for the segment stemming from alternative earthquake correlations, and (4) extend the earthquake record back to the early Holocene or latest Pleistocene for comparison with the records for the Brigham City and Salt Lake City segments.

RICE CREEK SITE

Rice Creek was the most promising site to investigate Holocene surface faulting on the rapidly urbanizing segment. We evaluated possible trench sites using geologic mapping by Nelson and Personius (1993) and Yonkee and Lowe (2004), analysis of the Weber segment earthquake history by Nelson and others (2006), our interpretation of 1:12,000- and 1:20,000-scale aerial photographs and 1-m-pixel digital orthophotos, unpublished scarp-profile data from A. Nelson (USGS; written communication, 2006), and field reconnaissance. We selected the Rice Creek site because two west-facing scarps have a simple geometry with 8 m and 4 m of vertical surface offset on an early(?) Holocene alluvial-fan surface (Nelson and Personius, 1993) and are not modified by younger alluvial-fan or landslide processes. These attributes are important for identifying the youngest surface rupture, obtaining the most complete Holocene earthquake record, and investigating a possible partial-segment rupture on the northern Weber segment.

Geologic Setting

The Rice Creek site is east of North Ogden, about 3 km south of the northern end of the Weber segment (figure 3). At the site, down-to-the-west surface faulting on two fault strands has displaced the apex of a Holocene alluvial fan that is incised into Bonneville shoreline deposits. We mapped the surficial geology of the site at 1:10,000 scale (figure 4) using low-sun-angle aerial photographs (Cluff and others, 1970), National Agriculture Imagery Program (ca. 2004) and USGS digital aerial photographs (ca. 1997), and survey-grade GPS (Trimble 5800). We also used survey-grade GPS to make a 0.5-m-contour-interval topographic map of the site and to measure profiles across fault scarps (figure 5). The topographic map shows the morphology of the faulted alluvial-fan surface, and the fault-scarp profiles yield scarp-height and net-surface-offset measurements (figure 6).

Late Pleistocene and Holocene surficial deposits at the Rice Creek site include hillslope and fault-scarp-derived colluvium, landslide deposits, stream and debris-flow deposits related to alluvial-fan deposition, and lacustrine deposits. Surface-faulting earthquakes have displaced most of these deposits, forming moderate (less than 5 m high) to large (greater than 10 m high) fault scarps and simple to complex fault traces (figure 4). The oldest surficial deposits are pre-Bonneville alluvial-fan deposits (af4, figure 4), which are exposed only in the footwall of the fault. Latest Pleistocene lacustrine (Lake Bonneville) and Holocene alluvial-fan deposits have buried corresponding deposits on the downthrown side of the fault.

The highstand shoreline of Lake Bonneville (Bonneville shoreline; figure 4) is used as a late Pleistocene time marker throughout the Bonneville basin. The lake occupied this

shoreline from about 15,500 to 14,500 ^{14}C yr B.P. (Oviatt, 1997; 18–17 ka [thousands of calendar-calibrated years B.P.]), when the lake level dropped catastrophically in response to erosion at its outlet at Zenda, Idaho. The lake stabilized about 100 m lower at the Provo level (occupied from about 14,500 ^{14}C yr B.P. [Oviatt, 1997] to ~12,000 ^{14}C yr B.P. [Godsey and others, 2005]; ~17–14 ka), which is below the elevation of the Rice Creek site. On the footwall of the WFZ south of the trench site, the Bonneville shoreline is expressed as a wave-cut bench on bedrock (now mostly covered by slope collu-

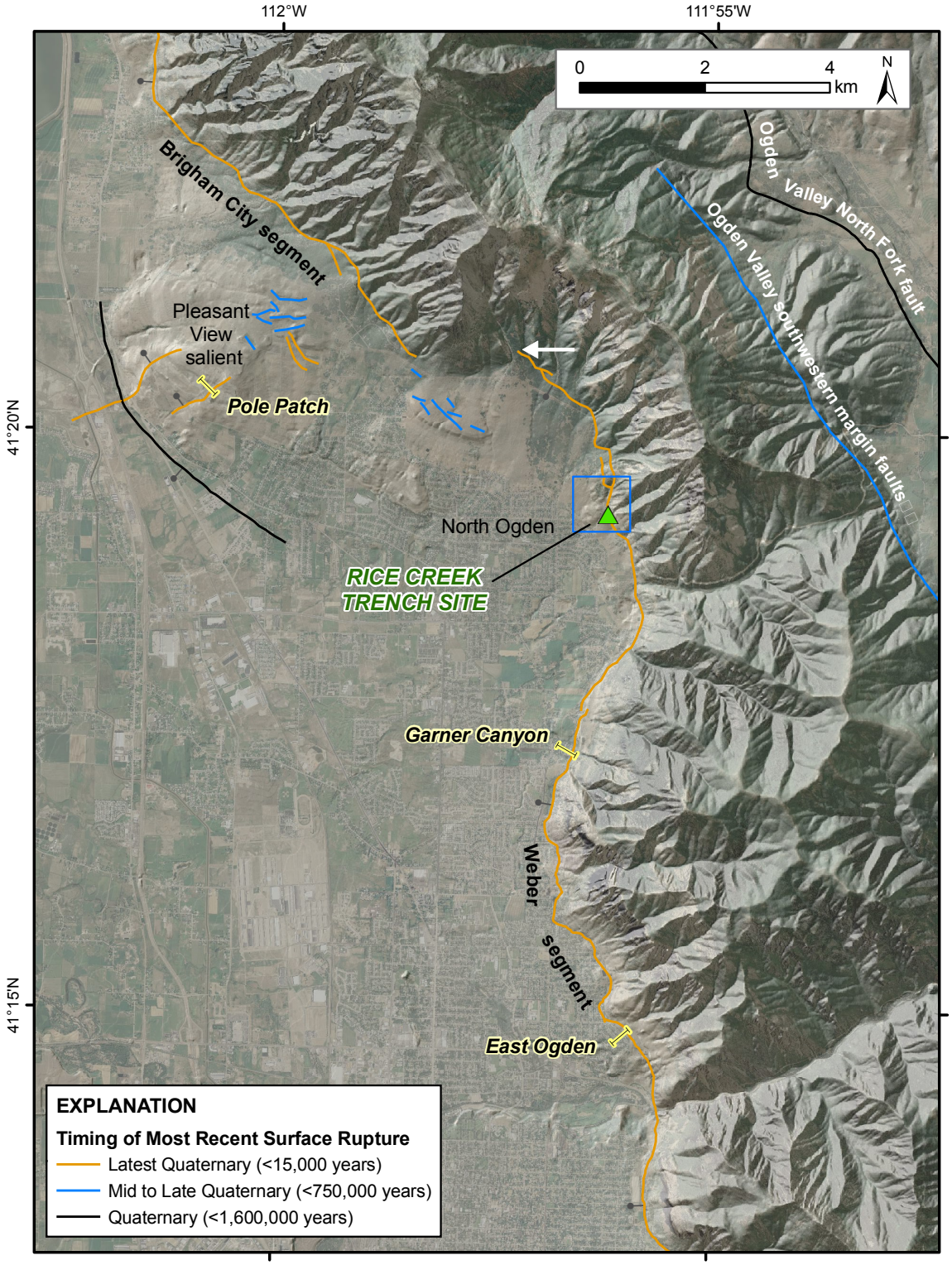

Figure 3. *Northern Weber segment. Fault-trace and timing data from Nelson and Personius (1993) and Black and others (2003); ball and bar on downthrown side of faults, white arrow indicates northern end of Weber segment. Box outlined in blue is extent of figure 4. Basemaps: National Agriculture Imagery Program aerial photography (U.S. Department of Agriculture, 2008) and 10-m digital elevation model.*

vium) at an elevation of about 1590 m (figure 7). About 200 m southeast of the site, Nelson and Personius (1993) mapped faulted nearshore sand deposits associated with the highstand shoreline and measured a vertical offset of 28 m across these deposits (figure 4).

Following the retreat of Lake Bonneville, alluvial fans dominated by reworked Lake Bonneville sand and gravel were deposited. Alluvial-fan deposition continued intermittently through the Holocene as mixed stream and debris-flow sediments issued from a steep, narrow, 0.3–0.4 km^2 drainage basin in the Wasatch Range (figure 3) to form well-defined alluvial-fan surfaces (af1 and af2; figure 4).

Scarps formed on Lake Bonneville lacustrine and alluvial-fan deposits provide evidence of multiple surface-faulting earthquakes on the WFZ along two down-to-the-west strands (figure 4). Two subparallel scarps on the Rice Creek alluvial fan mark these strands (figure 4): a 10-m-high (8-m-offset) upper scarp and a 6-m-high (4-m-offset) lower scarp (Nelson and Personius, 1993) (figures 5 and 6). A 0.4- to 0.6-m-high down-to-the-east antithetic scarp also offsets the alluvial-fan surface about 40 m west of the lower scarp.

Surface Offset

We measured surface offsets across the upper, lower, and antithetic scarps using the projections of alluvial-fan surface slopes from three fault-scarp profiles. To determine surface offset, we used profile points that best represented the pre-faulting alluvial-fan surfaces and yielded surface slopes of about 8–12° adjacent to the upper and lower scarps and about 9–10° east and west of the antithetic scarp (figure 5). Based on profile 1, which crossed the entire site, the upper scarp has 6.8 ± 0.8 m of surface offset and the lower scarp has 4.3 ± 0.3 m of surface offset (figure 6). Profiles 1, 2, and 3 cross the antithetic scarp and indicate 1.0 ± 0.4 m of surface offset (figures 5 and 6).

Three different approaches yielded net site surface offset estimates (figure 6). The offset between the uppermost alluvial-fan surface (east of the upper scarp) and surface between the lower and antithetic scarps is 10–11 m. Projecting the uppermost and lowermost (west of the antithetic scarp) surfaces toward the main scarps yields a surface offset of 9.4–12.0 m. The large uncertainty results from dissimilar surface slopes (uppermost 12º and lowermost 9º). The surface offset result-

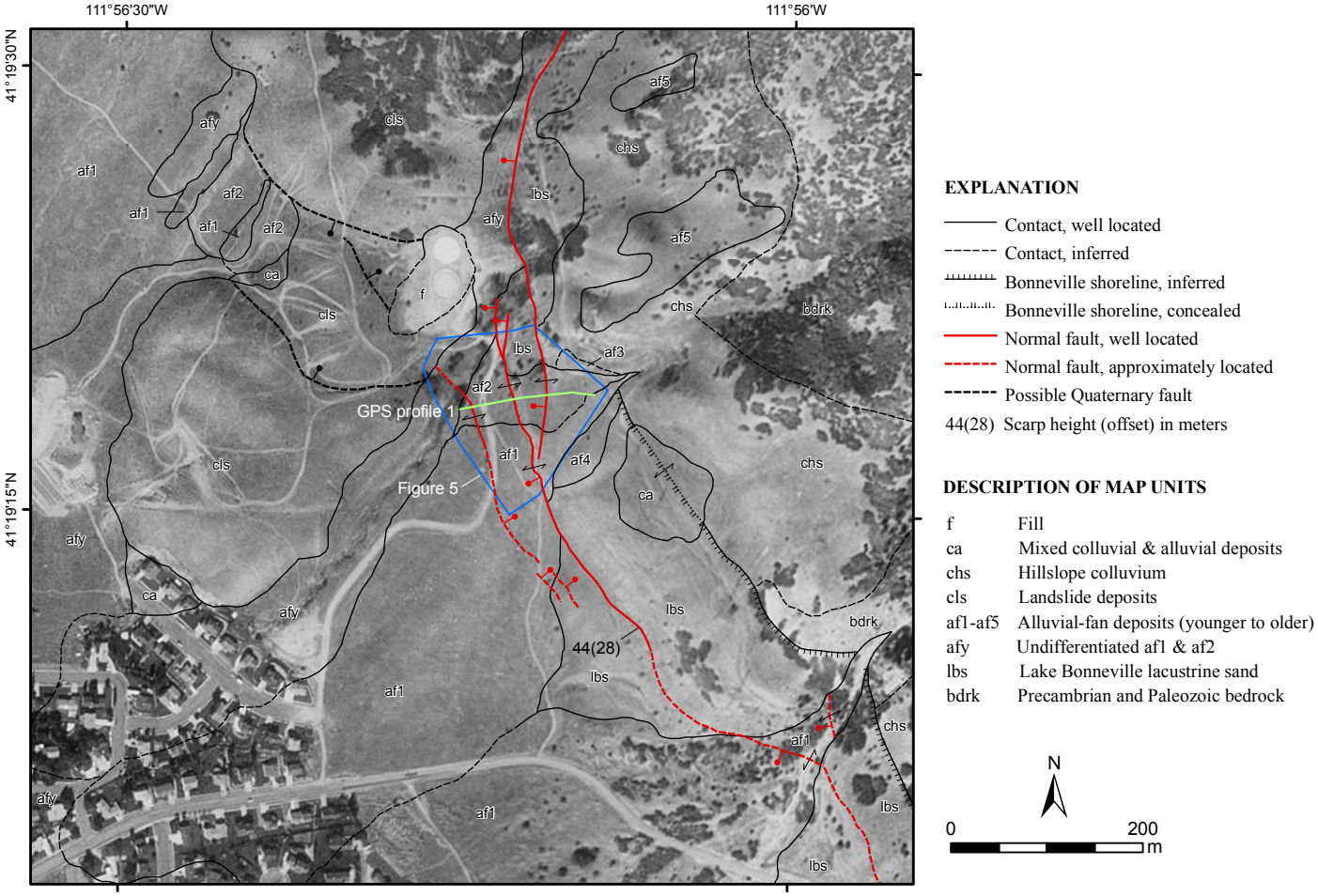

Figure 4. *Surficial geologic map of the Rice Creek site and surrounding area (this study); trace of the Wasatch fault shown in red; ball and bar on downthrown side. GPS profile 1 shown on figure 6. Base map is 1-m digital orthophoto (ca. 1997). Scarp height and offset data are from Nelson and Personius (1993).*

ing from summing the upper- and lower-scarp offsets (6.8 ± 0.8 m and 4.3 ± 0.3 m) and subtracting the antithetic-scarp offset (1.0 ± 0.4 m) is 8.6–11.6 m. Based on these estimates, the average net surface offset for the site is 9.3–11.5 m, where the lower bound (9.3 m) is the average of the minimum offset values (10, 9.4, and 8.6 m) and the upper bound (11.5 m) is the average of the maximum values (11, 12.0, and 11.6 m).

Trench Excavations

We excavated two trenches at Rice Creek: a 73-m-long main trench across alluvial-fan deposits faulted by the two main fault strands and a 7-m-long trench across the antithetic fault (plate 1). The main trench had a vertical south wall and benched north wall, and the shallower antithetic trench had two vertical walls. We mapped the stratigraphy at 1:20 scale for (1) the entire south wall of the main trench, (2) a 7-m-long section of the north wall of the upper fault zone in the main trench, and (3) both walls of the antithetic trench (plate 1). Using a total station (Trimble TTS 500), we measured the positions of nails along stratigraphic contacts and structures and projected the points to a vertical plane that was parallel to the average orientation of each trench wall. We then plotted the points for each wall on mylar and sketched in additional

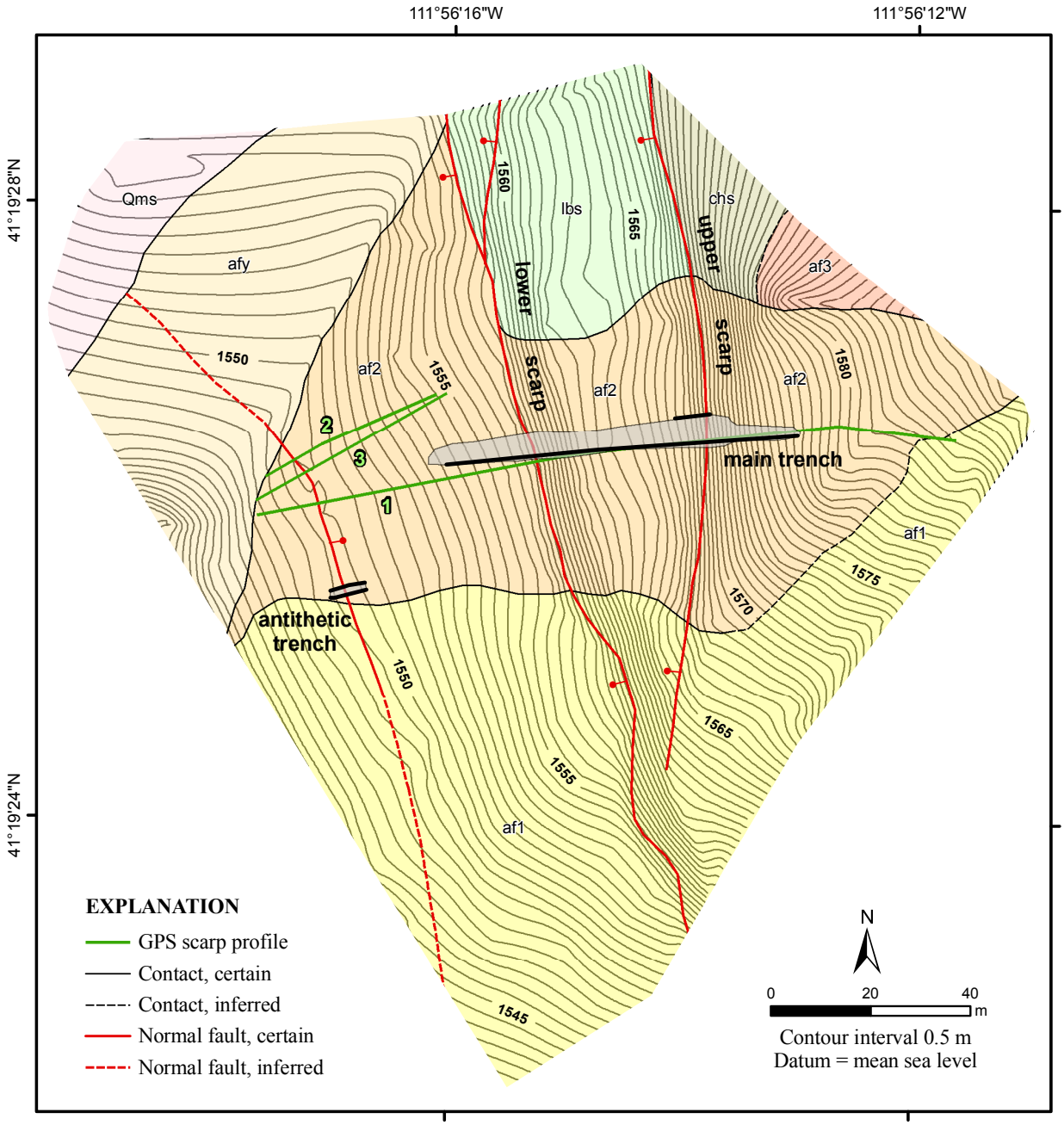

Figure 5. Topographic map of the Rice Creek site, showing excavated areas (light gray) and mapped trench walls (heavy black lines). Map generated using survey-grade GPS elevation data. See figure 4 for description of map units. Green lines indicate GPS scarp profiles 1, 2, and 3 (see figure 6).

detail in the fault zones. Plate 1 includes maps of the exposures with a coordinate system referenced in the discussion below as horizontal meter marks (h-) and vertical meter marks (v-) (e.g., h-33 m, v-3 m; plate 1). Photomosaics of the fault zones (1 m squares) in the main trench also show details of the trench walls (plate 1). Appendix A includes descriptions of the stratigraphic units identified in the trenches.

Radiocarbon Dating

Sampling and Dating Strategy

Because we did not find any macroscopic charcoal fragments in the trenches, we collected 26 liter-sized bulk samples of organic-rich sediment for radiocarbon dating from the upper 5-10 cm of A horizons developed on alluvial-fan (e.g., sample RC-C19; h-59 m, v-11.5 m; plate 1) and scarp-colluvial deposits (e.g., sample RC-C13; h-54.6 m, v-13.3 m; plate 1). The A horizons are 10–30 cm thick and composed of dark-brown silt-, clay-, and organic-rich sediment. We also collected 5- to 10-cm-thick samples of organic-rich sediment from the matrix of most colluvial deposits (e.g., sample RC-C18; h-59 m, v-11.6 m; plate 1). The colluvial-matrix samples are composed of fine-grained, dark-brown organic sediment that locally forms thin (2- to 10-cm-thick) lenses (h-52.5 m, v-14.5 m; plate 1). The organic matrix sediment has two probable origins: (1) organic-rich detrital sediment washed from A horizons uplifted and exposed in the footwall of the fault, or (2) cumulic A horizons formed in place, presumably due to wetter soil-moisture conditions associated with the fault zone. We did not map A horizons on the most organic-rich colluvial deposits (units 1 and 2; plate 1) because of discontinuous preservation of A horizons and the difficulty in differentiating them from the organic-rich matrix sediment.

We submitted 24 bulk samples of organic-rich sediment (C1 to C24; appendix B) to Paleo Research Institute for the separation and identification of plant macrofossils. Paleo Research Institute separated the samples into light (charcoal and plant

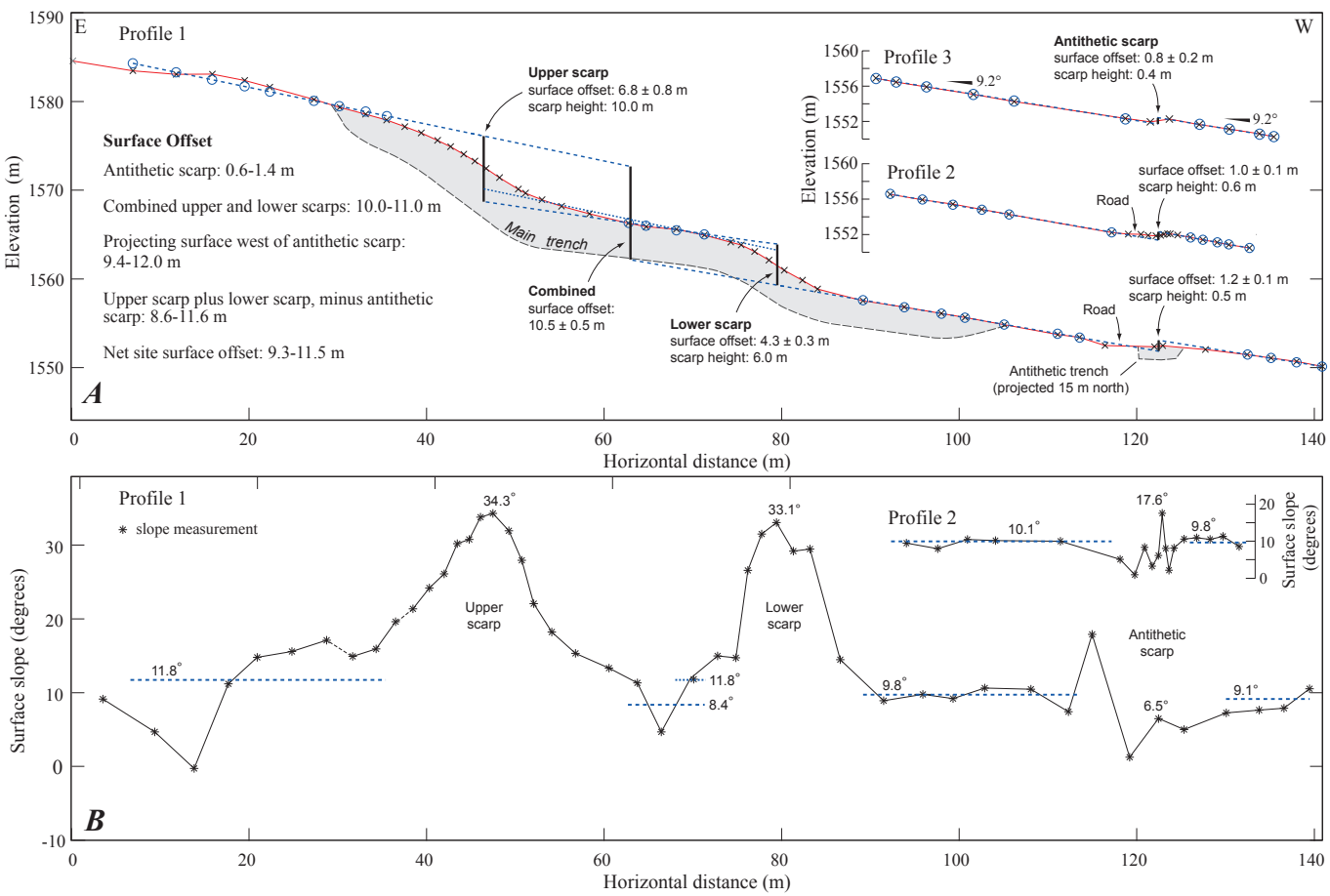

Figure 6. *Scarp-profile and surface-slope information for the Rice Creek site. (A) GPS scarp profiles, showing main- and antithetic-trench locations (shaded gray areas). See figure 5 for profile locations. Vertical surface offset (vertical black lines) calculated by projecting surfaces (dashed blue lines) toward fault scarps; scarp height is after McCalpin (1996). Profile points (x's) used for surface projections are indicated with blue circles. (B) Surface slope for profiles 1 and 2; slope values at peaks indicate maximum surface-slope angles for the upper, lower, and antithetic scarps; horizontal dashed blue lines and slope values indicate angles of projected surfaces used to calculate surface offset.*

Figure 7. *The Rice Creek site. (A) Upper and lower scarps; view is to the southeast. Yellow dotted line indicates approximate location of main trench. (B) Excavation of the main trench; view is to the east.*

remains) and heavy (sediment) fractions following the flotation methods of Matthews (1979) and then sieved and examined the light fractions for charcoal, seeds, and other plant remains under 10-70X magnification. Our preferred material for dating consisted of charred macrofossils of tree or shrub species local to the site that have short age spans (e.g., sagebrush; see Puseman and Cummings, 2005) and thus are less likely to have been transported long distances. This method is preferable to radiocarbon-dating techniques used in previous Weber-segment paleoseismic investigations (e.g., Nelson and others, 2006), which mostly relied on apparent mean residence time (AMRT) ages on bulk A-horizon sediment. AMRT ages are difficult to interpret because of the complex accumulation and decay of organic matter in the A horizon, and the potential for the sediment to contain younger carbon from root penetration or burrowing (Machette and others, 1992).

Our attempt to sample and date charcoal identified to family or genus level yielded mixed results because many of our bulk samples did not produce fragments of identifiable charcoal. Twelve of our bulk samples yielded charcoal fragments of an identified genus or family local to the site (Asteraceae [flowering plants], *Artemisia* [flowering plants such as sagebrush], *Quercus* [oak], *Juniperus* [juniper], and *Opuntia* [prickly pear cacti]; appendix B). Unfortunately, 13 of our bulk samples only yielded collections of small, unidentified charcoal fragments. For unidentified charcoal, multiple fragments were aggregated into samples of at least ~0.5 mg that yielded composite charcoal ages. The composite ages are averages of the charcoal fragments sampled from the A-horizon or colluvial sediment. Although detrital charcoal could have been present in either the unidentified or identified samples, the stratigraphic consistency of most ages with depth and the similarity between unidentified- and identified-charcoal ages from single A horizons (e.g., C3a, C3b, C4a, C4b) lend confidence to our results.

We submitted 24 charcoal samples to Woods Hole Oceanographic Institute for accelerator mass spectrometry radiocarbon dating. Sample pretreatment methods are summarized in appendix B. Radiocarbon ages (appendix B) are reported in calendar years before present (A.D. 1950) (cal yr B.P.), calibrated using the OxCal radiocarbon calibration program (v. 4.0; Bronk Ramsey, 1995, 2001, 2008) and the non-marine calibration dataset IntCal04 of Reimer and others (2004). Calibrated ages are reported as two-sigma ranges, although epistemic (model-based) sources of earthquake-dating uncertainty, such as the context of the sample (see below), likely far outweigh the analytical uncertainties (Nelson and others, 2006).

Sources of Dating Uncertainty

Samples derived from buried A horizons may yield anomalously young or old radiocarbon ages, despite having a known stratigraphic and structural context (Machette and others, 1992; McCalpin, 1996). Anomalously young ages (e.g., several hundred years or more younger than the average A-horizon age from additional samples) likely indicate burrowing or root mixing, which can transport young carbon from the modern A horizon at the ground surface to lower stratigraphic levels (e.g., sample RC-C7; h-21.7 m, v-27.8 m; north wall, plate 1). Radiocarbon ages from A-horizon sediment may also reflect the time span over which the soil formed. For example, samples from a modern A horizon may yield ages from zero to beyond the initial time of soil development. Anomalously old ages (several thousand years greater than the average A-horizon age) probably indicate carbon reworked from soils that predate the sampled A horizon (e.g., sample RC-C10; h-52.2 m, v-14.6 m; plate 1). To minimize these potential dating uncertainties, we avoided sampling near heavily burrowed parts of the trench exposure and collected the uppermost part of the A horizons to obtain the youngest carbon accumulated in the soil prior to burial.

Samples of colluvial-matrix sediment may also yield anomalously young or old ages due to inclusion of burrowed or detrital sediment, respectively. However, we sampled the colluvial deposits assuming that the organic sediment would (1) closely approximate the time of surface faulting, because the organics were eroded from A horizons exposed by surface faulting, or (2) post-date the time of surface faulting, if the charred organics were from A horizons developed on the post-earthquake colluvium. We mostly collected colluvial-matrix sediment from the base of each colluvial deposit to bracket the burial age of the underlying A horizon.

Luminescence Dating

Optically stimulated luminescence dating uses the cumulative, *in situ* natural radiation dose of minerals within sediment to estimate their time since last exposure to sunlight (Huntley and others, 1985). Ideally, sufficient mineral exposure occurs during deposition to effectively reset or zero the luminescence signal, and thus the luminescence age represents the time of sediment deposition (Aitken, 1994). If insufficient sunlight exposure occurs (for example, because of rapid deposition or the light-filtering effect of turbid water), the sediments may possess an inherited luminescence signal (Forman and others, 1991) and the age will only provide a maximum age for the deposit.

We collected six samples for conventional (multi-aliquot) luminescence dating from the main trench (appendix C), and submitted five samples to the USGS Luminescence Dating Laboratory and one to the Utah State University Luminescence Laboratory. The samples consisted of (1) discontinuous lenses of medium- to fine-grained and moderately to well-sorted sand in the alluvial-fan sediments (samples L1, L3, and L4; appendix C), (2) fine-grained sediment that may be weathered A or B horizons on fan deposits and colluvium (sample L5 and L6), and (3) the well-sorted matrix sand in a debris-flow deposit (sample L2). We measured the *in situ* dose of background radiation from potassium, thorium, and

uranium isotopes using a gamma-ray spectrometer; appendix C shows the sample saturation percent, total radiation dose rate, and equivalent dose. Luminescence ages are reported as the midpoint of two-sigma age ranges, in calendar years.

OxCal Modeling

We used OxCal radiocarbon calibration and analysis software (version 4.0; Bronk Ramsey, 1995, 2001; using the IntCal04 calibration curve of Reimer and others, 2004) to better constrain the time ranges of individual earthquakes. The OxCal program probabilistically models the time distributions of undated events (e.g., earthquakes) by incorporating stratigraphic ordering information for radiocarbon and luminescence ages from a depositional model with historical constraints (Bronk Ramsey, 2008). Earthquake time ranges from the models are reported with two-sigma (95.4%) confidence intervals.

RICE CREEK TRENCH INVESTIGATION

The Rice Creek fault trenches exposed (1) coarse-grained, gently west-dipping Holocene alluvial-fan sediments; (2) main, subsidiary, and antithetic normal faults that vertically displace these sediments; and (3) fault-scarp-derived colluvium deposited after surface-faulting earthquakes.

Stratigraphy

Alluvial-Fan Deposits

Alluvial-fan deposits consist of coarse-grained, poorly sorted stream and debris-flow deposits. In general, the matrix of the deposits contains abundant sand, which is likely derived from Lake Bonneville nearshore deposits that form a bench immediately above the trench site (figures 4 and 7). The fan deposits are generally massive, but locally contain discontinuous sand and gravel interbeds and lenses of well-sorted sand. Stratigraphic contacts dip gently westward (parallel to surface slope) and can be traced laterally for as much as 15 m. The deposits fine and become more laterally continuous toward the western part of the main trench. Fan deposits exposed in the footwall of the upper fault zone, between the fault zones, and on the hanging wall of the lower fault zone have the same origin and approximate age, based on similarities in geometry, texture, color, and degree of soil development formed on them at the surface.

Luminescence ages indicate that most of the exposed alluvial-fan deposits are mid- to early Holocene. Ages for sand lenses within the fan deposits range from 4770–8970 yr (luminescence sample L1; appendix C) to about 14,000 yr (10,660–16,160 yr, L3 and L4). The older ages (~14 ka) may be from sand grains that were reworked from adjacent Lake Bonneville nearshore deposits, but not completely reset by exposure to sunlight during erosion and deposition. The well-sorted sand matrix of a debris flow at the top of the fan sequence yielded a luminescence age of 2100–15,500 yr (L2). This sample's broad age range shows that most of its sand grains were not reset during deposition, and thus have highly variable inherited age components. About 3 m below the top of the alluvial-fan sequence, a fine-grained layer that may be a soil on intra-fan scarp colluvium (unit 5; plate 1) yielded a luminescence age of 7810–9930 yr (L6). A second sample from below the intra-fan colluvium yielded an age of 860–2180 yr (L5); however, this age is anomalously young considering the sample's stratigraphic position below all other luminescence samples and likely signifies that the sample was contaminated or exposed to light prior to processing.

Radiocarbon ages provide a minimum constraint on the age of the youngest alluvial-fan deposits. Charcoal from an A horizon developed on the youngest fan deposits in the lower fault zone (unit 4a; plate 1) yielded ages of 1590–1930 cal yr B.P. (radiocarbon sample C19; appendix B) and 3580–3830 cal yr B.P. (C15). In the upper fault zone, charcoal from an A horizon developed on the oldest scarp-derived colluvium (unit 3; plate 1) yielded four ages between 4520–4970 cal yr B.P. (C3b) and 5320–5600 cal yr B.P. (C3a, C4a, C4b).

The luminescence and radiocarbon ages indicate that the Rice Creek fan had a period of active, but likely intermittent, deposition between the early and middle Holocene. Luminescence samples L1 and L6 provide a maximum constraint on the age of the Rice Creek fan of 4.8–9.9 ka; radiocarbon ages for the A horizon on the oldest scarp colluvium in the upper fault zone provide a minimum age constraint of about 4.5–5.6 ka. Radiocarbon ages in the lower fault zone show that soil development (rather than fan deposition) on this part of the fan continued into the late Holocene. This is consistent with our geologic mapping (figure 4), which shows an Af2 (approximately mid-Holocene) fan surface at the trench site and a younger (~late Holocene) fan surface (Af1) to the south (figure 4).

Scarp-Derived Colluvium

Deposits of scarp-derived colluvium are locally derived from erosion of fault scarps formed during surface-faulting earthquakes. The colluvial deposits contain abundant sand and gravel, but also contain more silt, clay, and organic material than the alluvial-fan deposits. For colluvial units, we mapped a basal debris facies and an upper wash facies (after Nelson, 1992). The debris facies generally consists of coarse gravel and cobbles and soil blocks that accumulated at the base of the scarp resulting from erosion or collapse of the scarp free face. The wash facies is composed of sand, silt, and clay washed from the developing scarp slope, forming slope-parallel lenses (commonly with elongate clasts aligned parallel to the surface) that bury the debris facies and prograde out from it. Several meters downslope from the scarps, the individual wash-facies colluvial deposits coalesce. For example, downslope (west) of the upper scarp, a single 0.2- to 0.7-m-thick deposit

of undifferentiated slope wash extends laterally for a distance of about 15 m (plate 1).

Fault-Zone Geometry

The WFZ consists of three main fault zones formed in alluvial-fan deposits. We mapped two distinct down-to-the-west fault zones in the main trench: an upper fault zone and lower fault zone. On the hanging wall of the lower fault zone, a minor down-to-the-east antithetic fault zone was exposed in the antithetic trench (plate 1).

The upper fault zone coincides with the upper scarp and consists of a 5- to 6-m-wide zone that contains two west-dipping main faults (F1 and F2; plate 1) and two east-dipping antithetic faults (AF1 and AF2; plate 1). Well-developed (several-centimeter-thick) zones of shearing (unit 4s; plate 1) are most evident along faults F1, F2, and AF2. An east-dipping antithetic fault (AF3; h-38; plate 1) about 15 m west of the upper fault zone is associated with a minor uphill- (east-) facing scarp near the crest of the lower scarp, and has evidence for at least one surface-faulting earthquake.

The lower fault zone is about 30 m west of the upper fault zone and includes a complex, 11-m-wide zone of normal faulting associated with the lower scarp (plate 1). We mapped a main, west-dipping fault zone (F4; plate 1) composed of several fault strands that bound packages of sheared sediment (h-53 m, v-13 m; plate 1) and two antithetic faults (AF4; plate 1) that are buried by possible scarp colluvium (h-54, v-12; plate 1). The lower fault zone also includes a 3.5-m-wide graben about 6 m west of fault F4 (between faults F5 and AF5; h-57.5-61; plate 1).

In the antithetic trench, about 40 m west of the main fault in the lower fault zone (h-92-99; plate 1), a 2-m-wide antithetic fault zone is marked by a 0.5-m-high scarp. Faulting in this zone includes two down-to-the-east fault strands (AF6a and AF6b; plate 1). Although we were unable to correlate faulted alluvial-fan deposits in the antithetic zone with those in the two main fault zones, the antithetic fault zone is likely structurally linked to the lower fault zone at depth.

Surface Faulting at the Rice Creek Site

The trenches revealed abundant evidence of multiple surface-faulting earthquakes. The upper fault zone exposed scarp colluvium and faults from three earthquakes that post-date the alluvial-fan deposits exposed in the trench (post-fan). In the lower fault zone, colluvium and faults suggests one intra-fan earthquake, one earthquake that occurred during the late stages of alluvial-fan deposition, and two post-fan earthquakes. One or more of the upper, lower, and antithetic fault zones may have ruptured in past surface-faulting earthquakes. Thus, earthquakes are discussed and labeled (figure 8) from oldest to youngest for each fault zone. Earthquakes U3 (oldest), U2, and U1 (youngest) ruptured the upper fault zone; earthquakes L4 to L1 ruptured the lower fault zone; and earthquakes AL2 and AL1 ruptured the antithetic fault zone.

We constructed separate OxCal models for the upper and lower fault zones to help in (1) refining the earthquake times (and uncertainties) and (2) considering alternate earthquake correlations between the fault zones (e.g., earthquakes U1 and L2 may both represent the youngest earthquake at the site, earthquake 1; see Correlation of Earthquakes section). Where the limiting ages are more consistent and numerous (e.g., radiocarbon ages constraining earthquake L1), the models yield tightly constrained earthquake times. However, several earthquakes are constrained by few ages, or by only minimum- or maximum-limiting ages. We modeled the timing of those earthquakes using OxCal, but include the broadest uncertainties in our final interpretations. The OxCal models also helped us identify several radiocarbon ages that are stratigraphically inconsistent, possibly because the charcoal in the dated samples was eroded from faulted soils exposed higher in the slope and incorporated in the scarp-colluvial deposits.

Our estimates of per-event vertical displacement for the earthquakes are based on projecting surfaces and contacts into the fault zones (projection method; plate 2), graphically restoring fault movements (graphical method; plate 2), and in some cases comparing the cross-sectional areas of scarp colluvial deposits exposed in the trench. In the projection method, we measured the vertical separation of surfaces (e.g., the top of the alluvial fan) or depositional contacts by projecting them into linear fault projections. These values are compared with our graphical-restoration estimates, which we determined by sequentially retrodeforming trench stratigraphy by removing fault displacement and tilting from separate earthquakes.

Upper Fault Zone

Earthquake U3: The oldest earthquake in the upper fault zone—earthquake U3—displaced alluvial-fan deposits (unit 4b, plate 1) on an eastern main fault (F1, h-19 m; plate 1). Colluvium from earthquake U3 (unit 3 in the UFZ; plate 1) includes very coarse debris, which tapers downslope from fault F1, and has a light-colored and discontinuous A horizon developed on it. Based on the difference in thickness of unit 3 across antithetic fault AF2 (h-22.5 m, v-23 m; plate 1), it likely filled and spilled over the downslope edge of a 4-m-wide graben (h-18.5-22.5 m; plate 1). Unit 3 partially buries moderately well stratified alluvial-fan deposits as well as a distinct sand- and cobble-rich debris-flow deposit exposed at the surface in other parts of the trench. There is no soil on the buried alluvial-fan unit 4b, which suggests that earthquake U3 likely occurred shortly after fan deposition ceased (4.8–9.9 ka).

Four radiocarbon ages (C3a, C3b, C4a, and C4b) on juniper charcoal and unidentified charcoal fragments from the weak A horizon developed on unit 3 (plate 1) constrain the minimum

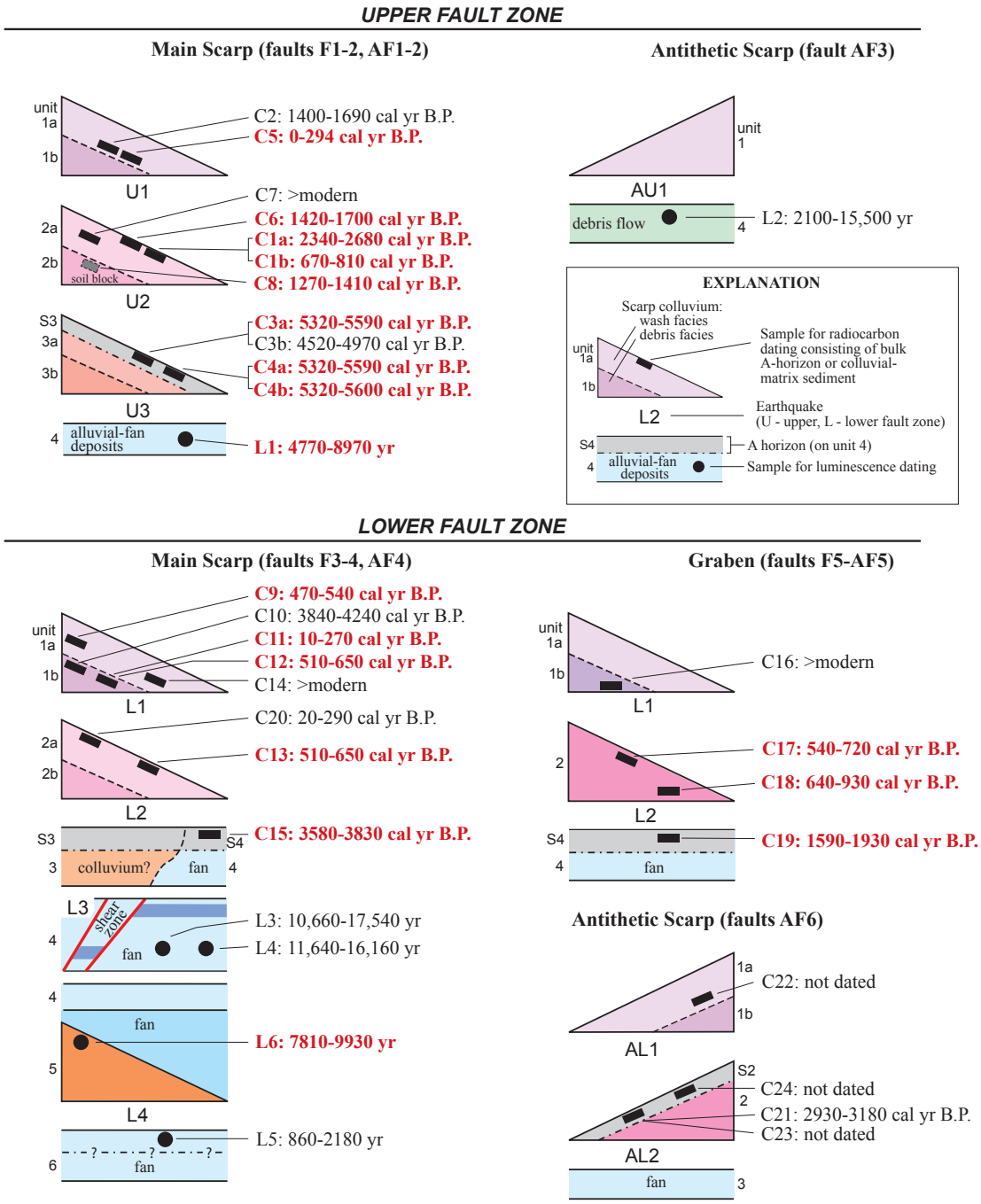

Figure 8. *Sampling strategy for the Rice Creek site. Triangles indicate colluvial wedges formed in response to paleoearthquakes (e.g., U1, L1); unit numbers correspond to plate 1. Radiocarbon and luminescence ages are two-sigma ranges; red bold text indicates ages used in our final interpretation of the Rice Creek paleoearthquake chronology (OxCal model D, figure 9; see text for discussion).*

time of earthquake U3 to 4520–5590 cal yr B.P. In addition, U3 is younger than the luminescence age of 4770–8970 yr (L1) for a moderately well sorted sand lens in the underlying alluvial-fan sequence. Luminescence sample L6 (7810–9930 yr) lies stratigraphically below sample L1 and also provides a maximum time for U3.

The U3 time range is 5500–7640 cal yr B.P. based on our OxCal modeling. Our model includes all luminescence and radiocarbon ages, with the exception of C3b, which is several hundred years younger than C3a, C4a, and C4b.

Earthquake U2: Surface faulting during earthquake U2 caused displacement on fault F1 and displaced colluvium from earthquake U3 (unit 3) on antithetic faults AF1 and AF2. Evidence for earthquake U2 includes organic-rich colluvium (unit 2; plate 1) composed of debris facies (unit 2b) and wash facies (unit 2a). Unit 2b buries the scarps formed by antithetic

faults AF1 and AF2 on the west side of a 6-m-wide graben (h-18.5-24.5 m; plate 1) and includes a distinct concentration of aligned cobbles at its base that lie directly on the weak A horizon formed on unit 3 (h-22 m, v-23 m; plate 1). Unit 2a consists of finer-grained and organic-rich sediment that may have a discontinuous A horizon developed on it.

Three charcoal ages (C1a, C1b, and C6) from the A horizon developed on unit 2a and one charcoal age (C8) from the matrix of unit 2b constrain the minimum time of earthquake U2 to 670–2680 cal yr B.P. The oldest age (2340–2680 cal yr B.P.; C1a) may be for detrital charcoal; however, the Asteraceae charcoal dated was likely derived from a plant local to the site and therefore we interpret the charcoal age as representative of the A-horizon age. Four radiocarbon ages from the A horizon developed on unit 3 limit the maximum time of U2 to 4520–5590 cal yr B.P.

The OxCal modeled time of earthquake U2 is 2460–5350 cal yr B.P. We excluded maximum age C3b (4520–4970 cal yr B.P.) considering its inconsistency with C3a, C4a, and C4b (5320–5590 cal yr B.P.). If C3b is included, the OxCal model produces a narrower time range for U2 of 2430–4680 cal yr B.P.

Earthquake U1: Earthquake U1 ruptured fault F2 (2-3 m west of fault F1; h-22.5, v-20.5; plate 1), displacing older colluvium (units 2 and 3) and antithetic faults. The unfaulted organic-rich colluvium associated with earthquake U1 (unit 1) consists of a small debris facies (unit 1b) and a laterally extensive slope-wash facies (unit 1a), both of which bury the possible A horizon developed on unit 2 (h-23.0, v-23.5 m; plate 1). Slope wash deposited after earthquake U1 (unit 1a) has buried the fault-scarp free face, but several meters downslope, unit 1a may include slope-wash sediment from earlier earthquakes. We could not identify individual subunits related to separate earthquakes.

Two charcoal samples from near the base of unit 1a provide minimum ages of 0–294 cal yr B.P. (C5) and 1400–1690 cal yr B.P. (C2) for the timing of earthquake U1. The age for sample C5 is anomalously young, likely from modern charcoal transported to the base of unit 1a through bioturbation. The older sample (1400–1690 cal yr B.P.; C2) may have contained charcoal eroded from a faulted soil previously exposed in the fault free face. The C2 age is older than the 670–810 cal yr B.P. (C1b) age for unit 2 A-horizon sediment, but consistent with the maximum ages of 1270–1700 cal yr B.P. (C6 and C8) from the unit 2 A horizon and matrix. Sample C1a (2340–2680 cal yr B.P.) provides an additional maximum time for U1. Given the three concordant ages (C2, C6, and C8) for the pre-earthquake U1 soil and the younger age for C1b, we prefer a maximum time of 1300–1700 cal yr B.P. for earthquake U1.

Two OxCal models constrain the time of earthquake U1: model A includes the maximum radiocarbon age of 670–810 cal yr B.P. (C1b) and model B does not. Model A indicates a U1 earthquake time of 170–760 cal yr B.P. Model B, which we prefer, indicates a broader time range of 210–1330 cal yr B.P. as it relies on the maximum ages of about 1300–1700 cal yr B.P. (C6 and C8). Sample C2 (1400–1690 cal yr B.P.) has a stratigraphically inconsistent age and is excluded from both models; all other ages constraining U1 are included.

Earthquake AU1: We do not have evidence to link antithetic surface faulting across fault AF3 (earthquake AU1) to upper fault zone earthquakes U1, U2, or U3. AU1 displacement probably occurred during earthquake U2 or U3 (or both) because of the lack of a buried soil on unit 4b-df (h-33-38 m; plate 1) below the antithetic-fault-zone colluvium (unit 1a; plate 1). In the upper fault zone, colluvium from earthquake U1 (unit 1) overlies a buried soil formed on colluvium from U2 (unit 2), but the underlying colluvium from U3 (unit 3) and alluvial-fan deposits (unit 4b) have little or no soil development.

Per-event displacement: Per-event displacements for earthquakes U3 and U2 average 1.6–2.3 m, which reflects the net displacement of alluvial-fan deposits and the fan surface across the UFZ (plate 2). Displacement on the antithetic fault AF3 (~1.0 m; h-38 m; plate 1) likely occurred before U1 (see above); however, we do not know how to apportion the displacement between U2 and U3, so it is divided equally between the two earthquakes. Accounting for displacement in U1 (1.4–1.6 m; discussed below) and the antithetic faulting, total displacement for U2 and U3 is 3.2–4.6 m, or an average of 1.6–2.3 m per earthquake. This estimate is similar to the per-event displacement of 2 m determined by graphical restoration (plate 2). Although the cross-sectional areas of the colluvium related to U3 (unit 3) and U2 (unit 2) suggest perhaps slightly more displacement in U2 (table 2), we did not use the area estimates to apportion displacement because unmapped colluvium from these earthquakes may be in the slope-wash-dominated unit 1a between faults F2 and AF3 (plate 1).

We estimate 1.4–1.6 m of vertical displacement for earthquake U1 (appendix A). This estimate is based on 1.5–1.6 m of vertical displacement of the contact between colluvial units from U2 (unit 2) and U3 (unit 3), as well as 1.4–1.5 m of down-to-the-west displacement of east-dipping antithetic faults associated with U2 (plate 2). The graphical restoration of U1 faulting indicates 1.6 m of net vertical displacement (plate 2).

The sum of per-event displacement estimates for the upper fault zone is 4.6–6.2 m, which is less than the vertical offset of 6.0–7.6 m from the scarp profile. The upper fault zone displacement is more consistent with the lower range of the scarp-profile offset (6 m), which is based on a steeper projection of the fan surface on the upper fault zone hanging wall, where it is not buried by scarp colluvium (h-40 to 70 m; plate 1). This estimate likely better represents the total offset displacement across the scarp because it is consistent with displacement estimates from both projection- and graphical-based methods.

Table 2. *Per-event vertical displacement estimates for the Rice Creek site.*

Earthquake[1]	Projection method (m)[2]	Graphical method (m)[3]	Area of scarp colluvium (m^2)[4]	Preferred displacement (m)
U1	1.4–1.6	1.6	5.4–9.3	1.4–1.6
U2	1.6–2.3	2.0	4.7–6.1	1.6–2.3
U3	1.6–2.3	2.0	3.6–4.5	1.6–2.3
L1	1.3–2.7	2.3–2.6	7.5	1.3–2.7
L2	1.3–2.1	1.6–1.7	2.5–4.5	1.3–2.1
L3	0.8–1.4	-	-	0.8–1.4
L4	>0.6–0.7	-	0.6	>0.6–0.7

[1] U, surface-faulting earthquake on upper scarp; L, earthquake on lower scarp.
[2] Vertical displacement per earthquake measured by projecting the surface of the alluvial fan and contacts between fan and colluvium subunits toward the fault zones (plate 2).
[3] Vertical displacement measured by incrementally removing per-event displacement and tilting (plate 2).
[4] Approximate cross-sectional area of scarp colluvium. For U1, minimum area is that measured above upper fault zone and maximum area includes colluvium between main fault and antithetic fault zones. For U2, U3, and L2, minimum area is actual mapped area, maximum area includes areas that we infer have been modified by later faulting (e.g., sheared or uplifted and eroded).

Lower Fault Zone

Earthquakes L4 and L3: The oldest surface-faulting earthquakes on the lower fault zone—earthquakes L4 and L3—occurred during a period of alluvial-fan deposition. Evidence for earthquake L4 includes colluvium (unit 5; h-51 m, v-14 m; plate 1) that buries west-dipping normal fault F3 about 1 m east of the most-recently active fault F4 (plate 1). Fault F3 displaces units 6-1 and 6-2 about 0.6–0.7 m down to the west. Unit 5 is interbedded with alluvial-fan sediments; it overlies a silt-rich horizon on unit 6-1 that may be a weathered soil (A horizon?) and is overlain by about 3 m of moderately well-bedded alluvial-fan deposits (unit 4b) that postdate earthquake L4. Fine-grained sediment near the top of unit 5 may indicate weak soil (A horizon?) development.

Earthquake L3 is defined by two well-developed, buried antithetic faults (AF4a and AF4b; plate 1) that displace a distinctive gravel bed (purple shading in unit 4a at h-55 m, v-12 m; plate 1) more than 0.8 m down-to-the-east (h-54.5 m, v-11.7 m; plate 1). These faults terminate upward at a gravel (unit 3) that may be a mixture of alluvial-fan and colluvial sediment deposited after erosion of the antithetic fault scarps. Following earthquake L3, an A horizon (s3 and s4; h-53.5-61.0 m; plate 1) developed on the alluvial/colluvial sediment (unit 3) and the faulted alluvial-fan deposits (unit 4a). Unit 3, which is at the top of the fan sequence in the hanging wall of fault F4, is younger than unit 5, which is buried several meters below the top of the fan in the F4 fault footwall.

The times of L4 and L3 are not well constrained by our ages (figure 8). Earthquake L4 is limited to a minimum of 7810–9930 yr, based on the luminescence age for a possible soil developed on unit 5 (L6, plate 1). Luminescence sample L5, from a possible faulted soil below unit 5, yielded an erroneously young age of 1520 yr and is not considered further here. Earthquake L3 occurred after deposition of alluvial-fan unit 4a-1 (h-56.5 m, v-12.5 m; plate 1), but before deposition of alluvial/colluvial unit 3 (h-54 m, v-13 m; plate 1). An A horizon is developed on unit 4a-1 that likely predates earthquake L3; however, this soil continued forming after earthquake L3 as it is also developed on unit 3. Thus, the unit 4a-1 A horizon both predates and postdates earthquake L3. Samples C15 and C19 are from the unit 4a-1 A horizon and yielded ages of 590–1930 cal yr B.P. (C19) and 3580–3830 cal yr B.P. (C15). We interpret the younger age for C19 as representing charcoal incorporated into the A horizon after earthquake L3, and thus providing a minimum time constraint. Charcoal from sample C15 is likely detrital, and therefore provides a maximum age for both unit 4a-1 and the timing of earthquake L3. Earthquake L3 is also constrained to a maximum time by luminescence ages of 7810–9930 yr (L6) for unit 5 and 4770–8970 yr (L1) for unit 4b-sd near the upper fault zone.

OxCal model C constrains the time of the three most-recent lower fault zone earthquakes (L3 to L1). We did not include earthquake L4 in the model because it only has a minimum-time constraint. Using radiocarbon samples C19 (1590–1930 cal yr B.P.) and C15 (3580–3830 cal yr B.P.) as minimum- and maximum-time constraints, L3 occurred at 1800–3660 cal yr B.P.

Earthquake L2: Earthquake L2 ruptured fault F4 (h-53 m; plate 1) and produced colluvial unit 2 that drapes faulted and fractured alluvial-fan deposits and the A horizon formed on units 3 and 4a in a 9-m-wide graben (between faults F4 and AF5; h-52-61 m; plate 1). Along fault F4, unit 2 was dragged upward during earthquake L1, forming a west-facing monocline (h-53.5 m, v-13.7 m; plate 1). Unit 2 thickens slightly toward fault F4, but we suspect that the most proximal (near-fault) part of the colluvium was incorporated into the F4 shear zone at h-52-53 m (plate 1). Extensive faulting and warping

of unit 2 limited our ability to differentiate between its debris and wash facies.

Three radiocarbon ages on charcoal from unit 2 young upward from 640–930 cal yr B.P. at the base to 510–650 cal yr B.P. near the top (samples C13, C17, and C18) and provide a minimum time for earthquake L2. A fourth sample from unit 2 yielded an anomalously young age of 20–290 cal yr B.P. (C20), and likely contained burrowed sediment. The maximum time of L2 is constrained by two charcoal ages of 1590–1930 cal yr B.P. (C19) and 3580–3830 cal yr B.P. (C15) from the A horizon developed on unit 4a-1 and buried by unit 2. The younger age (C19) likely represents a close maximum time for earthquake L2, whereas the older age for unidentified charcoal fragments (C15) is likely detrital and therefore indicative of the maximum age for the underlying alluvial sediment (unit 4a-1) rather than the age of the soil.

Earthquake L2 occurred at about 750–1730 cal yr B.P. based on OxCal model C, which includes the stratigraphically consistent radiocarbon ages from units 1 and 2 and the A horizon on the alluvial-fan surface (C9, C11, C13, C17, C18, and C19). The model excludes sample C20 (20–290 cal yr B.P), which has a near-modern age and may contain recently burrowed sediment, and sample C15, which probably dates the underlying alluvial unit 4a-1.

Earthquake L1: Evidence for earthquake L1 includes unfaulted colluvium (unit 1; plate 1) that buries both the well-developed shear zone along fault F4 (unit 4s; h-52.0-53.2 m; plate 1) and faulted and folded colluvium from earthquake L2 (unit 2; h-52.0 m, v-14.5 m; plate 1). Unit 1 is very loose, with organic-rich, slope-parallel gravel lenses, and distinct debris (unit 1b) and wash facies (unit 1a). Unit 1 includes sediment deposited in response to faulting on synthetic fault F5 (h-57.8 m; plate 1) that is about 5 m west of fault F4.

Radiocarbon-dated charcoal (C9, C11, C12, and C14) from the matrix of unit 1 (h-51.5-55 m; plate 1) defines a minimum time for earthquake L1 of 0–650 cal yr B.P. A fifth sample (C10) from unit 1 yielded a radiocarbon age of 3840–4240 cal yr B.P.; however, its unidentified charcoal fragments were probably reworked from older fan deposits exposed in the L1 free face following surface faulting. The maximum limit for L1 is from charcoal from the A horizon formed on unit 2. Three samples yielded ages of 20–290, 510–650, and 540–720 cal yr B.P. (C20, C13, and C17, respectively). We prefer the two 510–720 cal yr B.P. ages, which are consistent with four of the five ages from unit 1, and interpret the younger age (20–290 cal yr B.P.) as likely dating burrowed sediment. An additional radiocarbon sample from near the base of unit 2 (C18; plate 1) provides a loosely constrained maximum time of 640–930 cal yr B.P. for L1.

The time of earthquake L1 is 490–630 cal yr B.P. based on OxCal model C, which includes the four minimum ages from unit 1 (C9, C11, C12, and C14) and the two stratigraphically consistent maximum ages from unit 2 (C13 and C17). We did not include sample C10 (3840–4240 cal yr B.P.) from unit 1, based on its anomalously old age relative to samples from similar stratigraphic positions that cluster around 500–900 yr (figure 8). Sample C12 (510–650 cal yr B.P.) was also excluded because its age suggests the charcoal in the sample was eroded from a soil exposed in the L1 fault free face.

Earthquakes AL2 and AL1: The westernmost antithetic fault zone (AF6; plate 1) is about 40 m west of the lower fault zone (figure 5) and has evidence for two earthquakes: AL2 and AL1. Evidence for the older earthquake (AL2) consists of displacement of units 3a (south wall) and 3b (north wall) (h-93 m; plate 1) across antithetic fault AF6a and a small deposit of colluvium (unit 2) with an A horizon developed on it. Unit 2 overlies alluvial-fan units 3a and 3b, which show no soil development. In the south wall of the antithetic trench (plate 1), unit 2 has buried the AF6a fault scarp. The younger earthquake (AL1) displaced unit 3 and an A horizon formed on unit 2 on fault AF6b (but not AF6a). A small deposit of debris-facies colluvium (unit 1b) and a laterally continuous slope-wash colluvium (unit 1a) have partially buried the AF6b scarp.

Only one radiocarbon age constrains the time of surface faulting in the antithetic trench (figure 8). Charcoal fragments (C21) from an A horizon formed on unit 2, faulted by earthquake AL1, and buried by unit 1 (h-93 m, v-5.4 m; plate 1) yielded an age of 2930–3180 cal yr B.P. This single maximum age allows AL1 to be correlated with any of the three youngest surface-faulting earthquakes on the lower fault zone (L1, L2, or L3).

Per-event displacement: Earthquake L4 had a minimum displacement of 0.6–0.7 m. This estimate is based on the thickness of colluvial unit 5 (0.6 m) and 0.6–0.7 m of displacement across the top of unit 6-2 (plates 1 and 2), which is only exposed in the footwall of the lower fault zone (plate 1). We did not restore displacement from earthquake L4 because it occurred during active alluvial-fan deposition.

Our best estimate of displacement in earthquake L3 is 0.8–1.4 m. The minimum displacement accounts for a gravel lens faulted >0.8 m down-to-the-east across two antithetic faults (AF4a and AF4b), but presumably displacement during the earthquake primarily occurred on fault F4. The fault scarp formed by the antithetic faults has been completely eroded, so the thickness of alluvial/colluvial unit 3 (0.4–0.6 m) cannot be used to estimate displacement. However, displacement from earthquake L3 should be recorded in the total displacement for the lower fault zone. Thus, a reasonable average displacement for earthquake L3 is 1.3–1.4 m, determined by dividing the lower-fault-zone displacement of 3.8–4.1 m equally between L3, L2, and L1. We did not attempt to restore the displacement from L3, which likely occurred during active alluvial-fan deposition based on the restorations for earthquakes L2 and L1 (plate 2).

Earthquakes L2 and L1 resulted in 1.3–2.1 m and 1.3–2.7 m of vertical displacement, respectively (plate 2). These estimates are the maximum possible ranges of displacements determined by (1) dividing net displacement of the fan surface by two, (2) apportioning net displacement to the different earthquakes using relative scarp-colluvium area (table 2), (3) measuring and summing displacements separately for the main and subsidiary (synthetic and antithetic) faults, and (4) dividing net fan displacement by three, to account for L3 displacement. The projected alluvial-fan surface is displaced 3.8–4.1 m, which is similar to the scarp-profile surface offset of 4.0–4.6 m. We divide the lower fault zone displacement equally between L1 and L2 to obtain 1.9–2.1 m per event. However, if net displacement is apportioned using the cross-sectional areas of colluvium for these earthquakes (about 7.5 m^2 for unit 1 and 4.5 m^2 for unit 2; table 2), L1 displacement is 2.3–2.5 m (60%) and L2 displacement is 1.5–1.6 m (40%). In addition, using the individual main-fault displacement, 0.2-0.5 m of antithetic-fault movement in L2, and 0.5–0.6 m of synthetic faulting in L1, per-event displacement estimates are 2.5–2.7 m for L1 and 1.5-1.9 m for L2. The lower-bound estimate for L1 and L2 is 1.3–1.4 m, based on total lower fault zone displacement divided by three. The displacement estimates of 1.3–2.7 m for L1 and 1.3–2.1 m for L2 are the maximum possible ranges using the combination of these methods, which we prefer over the graphical-based estimates of 2.3–2.6 m for L1 and 1.6–1.7 m for L2 (plate 2), which do not account for separate displacement in earthquake L3.

The two surface-faulting earthquakes in the westernmost antithetic fault zone have a combined surface offset of about 1.0 m based on the scarp profiles (figure 6). Earthquake AL1 had 0.5–0.8 m of displacement, based on a displaced A horizon developed on both colluvium unit 2 and alluvial-fan unit 3b-1. Alluvial-fan deposits (e.g., 3a-2; plate 1) faulted in AL2 (but not in AL1) indicate about 0.2–0.3 m of displacement during AL2.

Correlation of Earthquakes

We considered alternate earthquake-correlation possibilities using the stratigraphic and chronological data, OxCal modeling results for the upper and lower fault zones, and per-event displacement estimates. Our preferred model (figure 9; appendix D) includes five earthquakes that occurred at the site between about 500 and 7500 cal yr B.P. A sixth earthquake (not included in the model) occurred before 7810–9930 yr (figures 9 and 10; tables 3 and 4).

Earthquakes 6 and 5 are based on evidence of surface faulting in earthquakes L4 and U3, respectively. Earthquake 6 occurred before 7810–9930 yr, but is not included in our OxCal models as it is only constrained by a single minimum age. Earthquake 5 is constrained to 5500–7530 cal yr B.P. by OxCal model D, which uses three minimum radiocarbon ages and two maximum luminescence ages (figure 10). Although the older end of the earthquake 5 time range (7530 cal yr B.P.) is close to the younger time limit for earthquake 6 (>7810 yr), colluvium deposited after earthquake 5 (U3) lies on top of the alluvial-fan sequence, whereas colluvium deposited after earthquake 6 (L4) is buried by several meters of fan deposits.

We interpret earthquakes L3 and U2 as evidence of two earthquakes at the site: earthquake 4 (U2) at 3690–5370 cal yr B.P. and earthquake 3 (L3) at 1790–3670 cal yr B.P. (OxCal model D, figure 10). Earthquake 4 likely occurred only on the upper fault zone (earthquake U2), before a 2340–2680 cal yr B.P. (C1a) age from colluvial unit 2, but after three nearly identical radiocarbon ages of 5300–5600 cal yr B.P. from two different samples of the buried A horizon on colluvial unit 3 (C3 and C4; figure 8). We interpret these concordant ages as close maximum times for earthquake 4 and therefore, as evidence that it occurred about 1500 yr before earthquake 3. Earthquake 3 may have only caused displacement on the lower fault zone (earthquake L3). Earthquake 3 occurred before the 1590–1930 cal yr B.P. (C19) age for the A horizon developed on unit 4a-1, and is probably constrained to a maximum of 3580–3830 cal yr B.P. (C15) from the detrital charcoal from unit 4a-1. A broader maximum age of about 4770–9930 yr is indicated from luminescence ages (L1 and L6) on underlying fan sediment.

Earthquakes 2 and 1 occurred at 750–1350 cal yr B.P. and 490–630 cal yr B.P. based on lower fault zone earthquakes L2 and L1, respectively. We also correlate earthquake 2 with upper fault zone earthquake U1 (figures 9 and 10). This interpretation is based on the similarity of radiocarbon ages that constrain U1 and L2 to less than about 1300–1700 yr, in contrast to L1 timing of ~500–600 yr. In addition, U1 and L2 have the smallest per-event displacements per fault zone, consistent with simultaneous faulting on both the upper and lower fault zones during earthquake 2. However, the radiocarbon ages also support an alternative scenario in which U1 correlates with earthquake 1 (and thus L1). In this scenario, sample C1b (670–810 cal yr B.P.) from the upper fault zone would provide an additional maximum constraint for earthquake 1, but have little effect on the timing of earthquakes 1 or 2.

RICE CREEK EARTHQUAKE PARAMETERS

Earthquake Timing and Displacement

At least five, and probably six earthquakes occurred at the Rice Creek site. Using stratigraphic and structural relations, radiocarbon and luminescence dating, and OxCal modeling (figure 9), our preferred scenario consists of six Holocene earthquakes (6 to 1; table 5, figure 11). Earthquake 6 occurred before 7810–9930 yr, during a period of active alluvial-fan deposition, and had a minimum of 0.6–0.7 m of vertical displacement in the lower fault zone. Earthquake 5 faulted the

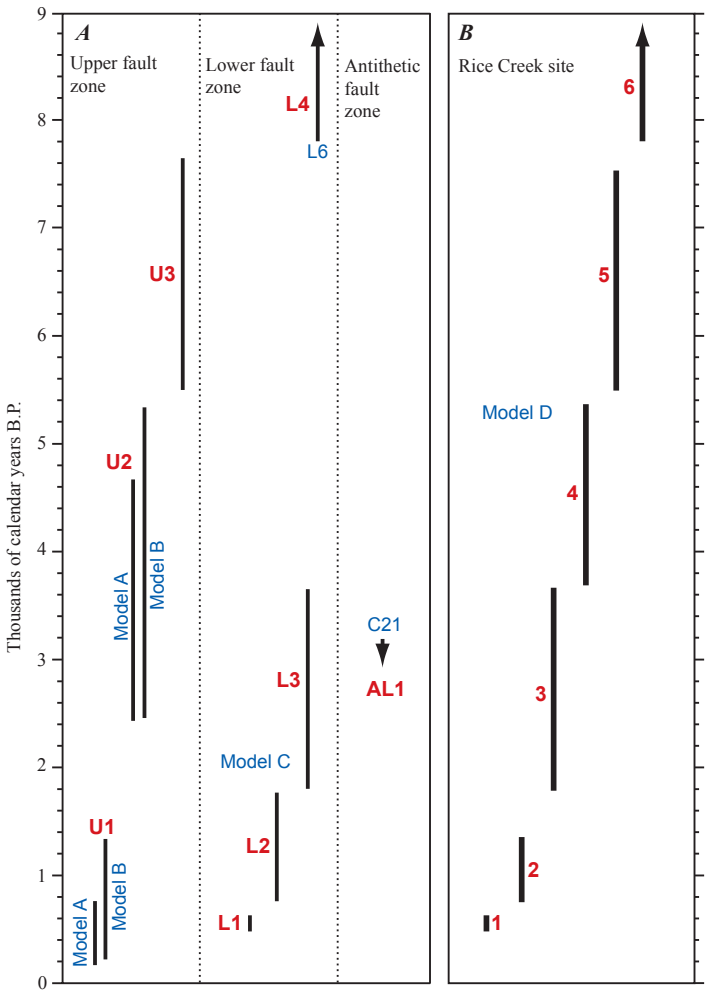

Figure 9. *Earthquake time ranges (two-sigma) for (A) the upper, lower, and antithetic fault zones, based on OxCal models A, B, and C; earthquakes L4 and AL1 are based on individual numerical ages (sample numbers indicated); and (B) the Rice Creek site as a whole, based on our correlation of upper and lower fault zone earthquakes (OxCal model D). See text for discussion of OxCal models, event correlations, and earthquake times.*

ground surface 1.6–2.3 m at 5500–7530 cal yr B.P., shortly after alluvial-fan deposition near the upper fault zone ceased. Although the two-sigma time ranges for these earthquakes overlap, stratigraphic and structural data clearly indicate two separate earthquakes. In our preferred OxCal model (D, figure 10), earthquakes 4 and 3 occurred as separate events at 3690–5370 cal yr B.P. and 1790–3670 cal yr B.P., respectively, with 1.6–2.3 m (4) and 0.8–1.4 m (3) of displacement. There is substantial structural and stratigraphic evidence for earthquake 4; however, poor timing information for earthquake 3 leaves ambiguity regarding whether earthquake 3 is in fact a separate earthquake. Strong stratigraphic and chronologic evidence indicate that the youngest earthquakes occurred at 750–1350 cal yr B.P. (earthquake 2) and 490–630 cal yr B.P. (earthquake 1). Earthquake 2 caused 2.7–3.7 m of vertical displacement, based on correlation of surface faulting in the upper and lower fault zones, and earthquake 1 had 1.3–2.7 m of displacement in the lower fault zone.

Displacement estimates for Rice Creek earthquakes 6 to 1 (table 5) are composite values based on per-event estimates per fault zone (table 2) and the correlation of earthquakes at the site (table 3). Per-event displacements for earthquakes 5 to 1 average 1.6–2.5 m. Earthquake 2 had the largest displacement (2.7–3.7 m), which is the sum of individual displacements for U1 (1.4–1.6 m) and L2 (1.3–2.1 m) (table 2). Earthquakes 3 and 6 had smaller displacements of 0.8–1.4 m and >0.6–0.7 m. The sum of the individual post-fan displacements (i.e., earthquakes 5 to 1) is 8.0–12.4 m, which is similar to the net surface offset of 9.3–11.5 m from scarp-profile data.

Our preferred net displacement of 8.0–12.4 m considers the per-event displacement, total site displacement, and scarp-profile surface offset. Net site vertical displacement is 8.0–12.4 m based on the sum of the per-event displacements for the post-fan earthquakes, 8.5–11.4 m based on projections of the uppermost and lowermost fan surfaces exposed in the main trench, and 9.5–9.9 m based on graphical trench reconstruction (plate 2). These estimates do not account for antithetic displacements in AL1 and AL2. Scarp-profile data that

Table 3. *Correlation of earthquakes at the Rice Creek site.*

Earthquake	Upper (U) fault zone (cal yr B.P.)[1]	Lower (L) fault zone (cal yr B.P.)[1]	Antithetic (A) fault zone (cal yr B.P.)[2]
1	**170–760 (U1)[a]**	**490–630 (L1)**	<2900–3200 (AL1)
2	**210–1330 (U1)[a]**	**750–1730 (L2)**	<2900–3200 (AL1)
3	**-**	**1800–3660 (L3)[b]**	<2900–3200 (AL1)
4	**2430–4680 (U2)**	**-**	-
5	**5500–7640 (U3)**	**-**	-
6	-	>7810–9930 (L4) [c]	-

[1] Summary of two-sigma earthquake time ranges. Bold text indicates time ranges based on separate upper and lower fault zone OxCal models (appendix D). [a] The two time ranges for earthquake U1 reflect separate OxCal models; in the preferred timing scenario and combined OxCal model D (figure 9) we prefer the broader (210–1330 yr) time range and interpretation that surface faulting in U1 occurred in earthquake 2 (see text for discussion). [b] Minimum time constraints for L3 are not considered in the lower fault zone OxCal model, but are used in the combined model D. [c] Based on luminescence age for sample L6 (appendix C), reported in calendar years.
[2] Maximum earthquake time (based on radiocarbon sample C21; appendix B) for antithetic fault zone earthquake AL1, which could correlate with earthquakes 1, 2, or 3.

account for the antithetic faulting suggest a net surface offset of 9.3–11.5 m, based on the projection of fan surfaces toward the upper and lower scarps and the sum of individual offsets for each of the upper, lower, and antithetic scarps (plate 1).

Minor differences in total displacement and net surface offset are likely related to the difficulty of projecting two-dimensional exposures of non-planar alluvial-fan surfaces tens of meters toward the upper and lower fault zones (plate 1). For example, the scarp-profile-based offset that includes the antithetic fault displacement is slightly different from the projection- and graphical-based displacement estimates, partly due to minor differences in fan-surface slope. The slope of the westernmost fan surface (west of the antithetic fault zone) is slightly shallower than the fan surface east of the antithetic fault zone and west of the lower fault zone. Projecting these surfaces toward the main scarps results in a larger surface-offset estimate for the westernmost fan surface than the surface between the antithetic fault zone and lower fault zone. Additionally, the larger net scarp-profile offsets may indicate a minor component of folding during surface faulting (e.g., near-fault tilt or warping) that is captured in the profile measurements but not in the individual event restorations.

Earthquake Recurrence and Vertical Slip Rate

Our best estimate of the mean Holocene recurrence interval at the site is 1500 yr based on the 1220–1760 yr range for the four intervals between earthquakes 1 and 5 (elapsed time of 4870–7040 yr). The two-sigma range (500–3100 yr) reflects the two-sigma recurrence interval ranges determined using OxCal (model D; appendix D). The interval between earthquakes 1 and 2 is the shortest (~500 yr), whereas the three two-sigma intervals between earthquakes 2 and 5 are more consistent at <2700–3300 yr, which is also consistent with the midpoint of the open-ended interval between earthquakes 5 and 6 (>2400 yr).

Per-event displacement divided by the previous recurrence interval yields a per-event vertical slip rate (table 5; appendix E). For example, the per-event slip rate between earthquake 2 and 1 is 1.6–14.2 mm/yr, based on 1.3–2.7 m of displacement in earthquake 1 divided by the 190–810 yr recurrence interval between these earthquakes. The per-event slip rates range from 0.2 to 14.2 mm/yr and average 0.7–7.9 mm/yr, using the two-sigma recurrence estimates. The very high slip rates (~8-14 mm/yr; table 5) reflect the poorly constrained lower bounds of the two-sigma recurrence intervals (200-600 yr; table 5) and are not considered further here.

Considering the uncertain earthquake recurrence times, the average vertical slip rate for the site may be a more stable approximation of fault activity. The average slip rate is the total site displacement (calculated from projected contacts/surfaces, graphical restoration, and scarp profile offset) divided by either the elapsed time between earthquakes (e.g., between earthquakes 6 and 1) or the age of the alluvial-fan deposits (appendix E). Based on the displacements calculated from the three methods noted above, our best estimate of the average vertical slip rate is 0.9–2.1 mm/yr. The slip rate based on the elapsed time of 7.2–9.4 kyr between earthquakes 6 and 1 is 0.9–1.6 mm/yr, which is an average rate that includes the minimum interval between earthquakes 6 and 5 but not the open interval from earthquake 1 to the present. The slip rate is 0.9–2.7 mm/yr when the total site displacement is divided by the 4.2–9.4-kyr interval between the approximate age of the alluvial fan (4.8–9.9 ka based on L1 and L6) and the time of earthquake 1 (490–630 cal yr B.P.).

Table 4. *OxCal output for model D.*

OxCal model D[1]	Unmodeled (cal yr B.P.)[2]		Modeled (cal yr B.P.)[3]		Agreement Index (%)[4]
	Min	Max	Min	Max	A
Sequence					
C_Date L6, 8870±1100	7760	9880	6990	9160	65.9
C_Date L1, 6870±1050	4720	8920	5910	8350	117
Earthquake 5			**5500**	**7530**	
Phase: soil on U3 colluvium					
R_Date C3a, 4750±40	5320	5590	5320	5590	99.7
R_Date C4a, 4730±45	5320	5590	5320	5590	99.6
R_Date C4b, 4770±50	5320	5600	5320	5600	100.1
Earthquake 4			**3690**	**5370**	
R_Date C15, 3430±35	3580	3830	3580	3830	99.8
Earthquake 3			**1790**	**3670**	
Phase: U2 colluvium					
R_Date C19, 1830±65	1570	1920	1570	1900	99.9
R_Date C6, 1650±35	1410	1690	1410	1690	99.8
R_Date C8, 1440±40	1290	1400	1290	1410	98.7
Earthquake 2			**750**	**1350**	
R_Date C18, 835±85	660	930	670	920	105.4
R_Date C17, 700±35	560	700	560	700	110.7
R_Date C13, 560±35	510	650	520	650	98
Earthquake 1			**490**	**630**	
Phase: L1 colluvium					
R_Date C9, 460±30	480	540	470	540	96.5
R_Date C11, 105±35	10	270	90	280	97.2
C_Date Historical constraint	100	110	100	110	100

[1] Phase indicates a group of ages with unspecified stratigraphic positioning. R_Date represents a radiocarbon age; C_Date is a calendar (e.g., luminescence) age. See appendix D for source code and text for discussion of the radiocarbon and luminescence ages included in the final model.
[2] Unmodeled ages are 2-sigma age distributions (rounded to the nearest decade) for prior (pre-modeling) probability density functions (PDFs), using calibration data from Reimer and others (2004).
[3] Modeled ages are 2-sigma ranges (rounded to the nearest decade) for posterior (post-modeling) PDFs using the stratigraphic ordering information. Earthquakes are treated as undated events in the model, and are thus assigned 2-sigma modeled ages based on the stratigraphic model.
[4] The agreement index (A) indicates agreement between probability density functions for unmodeled and modeled radiocarbon and luminescence ages. Agreement is poor below 60%. Agreement for the entire model is 93%.

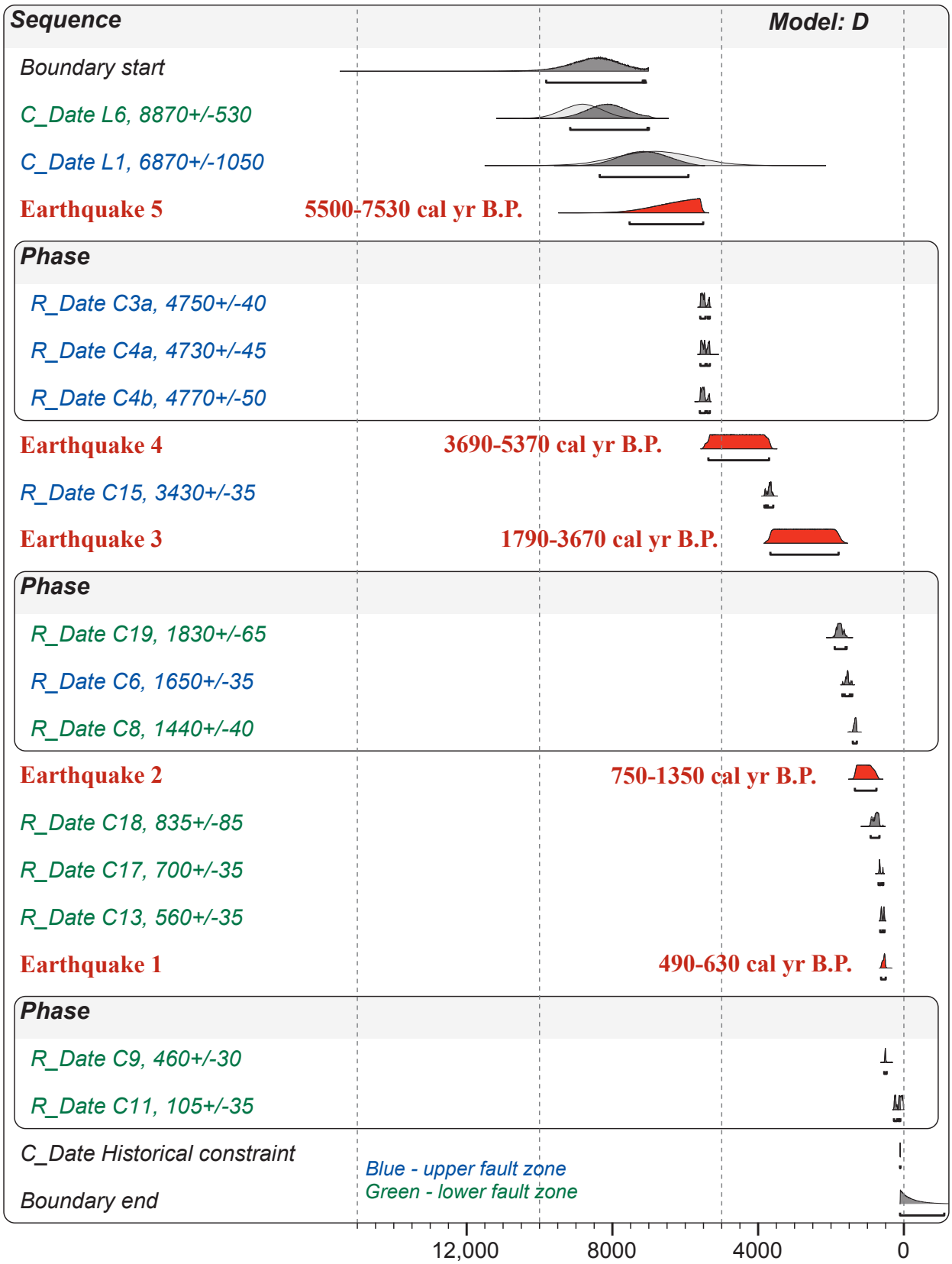

Figure 10. *Stratigraphic ordering and numerical control for the Rice Creek site, using OxCal v. 4.0 (Bronk Ramsey, 2001, 2008; Reimer and others, 2004), showing probability density functions for radiocarbon and luminescence ages and the modeled paleoearthquake time ranges (two-sigma) (appendix D). Light-gray-shaded areas represent prior (pre-modeling) distributions. Dark-gray-shaded areas indicate posterior (modeled) distributions using stratigraphic ordering information. Horizontal bars below distributions show two-sigma age ranges for posterior distributions.*

Table 5. *Summary of earthquake parameters for the Rice Creek site.*

Earthquake	Preferred timing (cal yr B.P.)[1]	Recurrence time (yr)[2]	Displacement (m)[3]	Interval slip rate (mm/yr)[4]
1	490–630	Earthquake 1-2: 190–810	1.3–2.7	1.6–14.2
2	750–1350	Earthquake 2-3: 620–2710	2.7–3.7	1.0–6.0
3	1790–3670	Earthquake 3-4: 380–3270	0.8–1.4	0.2–3.7
4	3690–5370	Earthquake 4-5: 320–3300	1.6–2.3	0.5–7.2
5	5500–7530	Earthquake 5-6: >280–4430	1.6–2.3	<0.4–8.2
6	>7810–9930[a]	-	>0.6–0.7	-

[1] Preferred earthquake timing reported at 95.4% uncertainty; based on OxCal model D (figure 9; appendix D). [a] Based on luminescence age for sample L6, reported in calendar years.
[2] Two-sigma recurrence intervals, modeled using OxCal model D (appendix D).
[3] Per-earthquake vertical displacement (plate 2; see text for discussion).
[4] Interval slip rate determined by dividing per-event vertical displacement by the previous recurrence interval (e.g., earthquake 1 displacement [1.3–2.7 m] divided by the recurrence time between earthquakes 1 and 2 [190–810 yr]).

DISCUSSION OF RESULTS

Our Rice Creek earthquake chronology corresponds well with the Kaysville, East Ogden, and Garner Canyon trench results, which are the basis for the consensus times of the Utah Quaternary Fault Parameters Working Group (UQFPWG; Lund, 2005) (figure 11). Importantly, we identified a previously unknown sixth earthquake on the segment at >7.8–9.9 ka. Rice Creek earthquakes 5 (5.5–7.5 ka) and 4 (3.7–5.4 ka) suggest that the earliest earthquake at Kaysville (X) at 3.8–7.9 ka (preferred range of 5.7–6.1 ka; McCalpin and others, 1994) is likely an older and separate earthquake from the earliest East Ogden earthquake (A) at 2.8–4.8 ka (table 1; figure 11). Earthquake 3 (1.8–3.7 ka) corresponds well with Kaysville earthquake Y (2.1–3.5 ka), East Ogden earthquake B (2.4–3.9 ka), and Garner Canyon earthquake B (1.4–2.8 ka). Earthquake 2 constrains the penultimate Weber-segment earthquake to 0.8–1.4 ka, consistent with estimates of 0.6–0.8 ka, 0.5–1.7 ka, and 0.6–1.5 ka from Kaysville, East Ogden, and Garner Canyon, respectively. Our preferred times for earthquakes 1 and 2 correspond well with and refine the time ranges of Lund (2005), whereas earthquakes 3, 4, and 5 are similar to the Lund (2005) estimates, but have broader ranges (figure 11).

Paleoseismic data from the Rice Creek site substantiate the ~500-yr earthquake found at the East Ogden site, 9 km to the south. Earthquake 1 at Rice Creek occurred at about 500–600 cal yr B.P., and likely correlates with East Ogden earthquake D, which occurred at 200–600 cal yr B.P. The youngest earthquakes at the Kaysville (600–800 cal yr B.P.) and Garner Canyon (600–1500 cal yr B.P.) sites (figure 11) likely correlate with older earthquakes at Rice Creek (earthquake 2, 750–1350 cal yr B.P.) and East Ogden (C, 500–1700 cal yr B.P.). Vertical-displacement estimates for the ~500-yr Rice Creek and East Ogden earthquakes decrease from 1.3–2.7 m at Rice Creek to 0.5–0.8 m at East Ogden (Nelson and others, 2006). McCalpin and others (1994) found no evidence for a ~500-yr earthquake at Kaysville on the southern half of the segment. The southward-decreasing displacement data may indicate that the 500-yr earthquake ruptured only the northern part of the Weber segment, which has important implications about how surface-faulting earthquakes should be modeled for Weber-segment hazard assessments.

Our Rice Creek paleoseismic data help refine earthquake-recurrence information for the northern Weber segment. Our best estimate of the mean recurrence time between large earthquakes during the Holocene is 1500 yr with an estimated two-sigma range of 500–3100 yr, based on our preferred scenario of six Holocene earthquakes. This estimate includes the relatively short recurrence interval of ~500 yr between earthquakes 1 and 2, which may be due to a partial-segment rupture of the northern part of the segment, as well as the three more consistent intervals between earthquakes 2 and 5. Our preferred recurrence-interval range is similar to the Nelson and others (2006) estimate of ~1500–1600 yr (0-3000-yr possible range), based on the two intervals between Weber-segment earthquakes A and C (table 1). The UQFPWG (Lund, 2005) estimated a recurrence interval of 1400 yr (500-2400-yr estimated two-sigma range), which accounts for the four intervals between the five most-recent earthquakes (table 1). Our longer upper limit stems from the weighted average of the two-sigma ranges between earthquakes 1 and 5.

Per-event- and total-displacement estimates contribute to our preferred vertical-slip-rate estimate of 0.9–2.1 mm/yr. Our preferred net displacement for the site is 8.0–12.4 m, based on a combination of scarp-profile data, projections of stratigraphic contacts and geomorphic surfaces, graphical reconstruction of faulting, and correlation of surface-faulting earthquakes between the upper and lower fault zones. Per-event displacements average 1.6–2.5 m (excluding earthquake 6

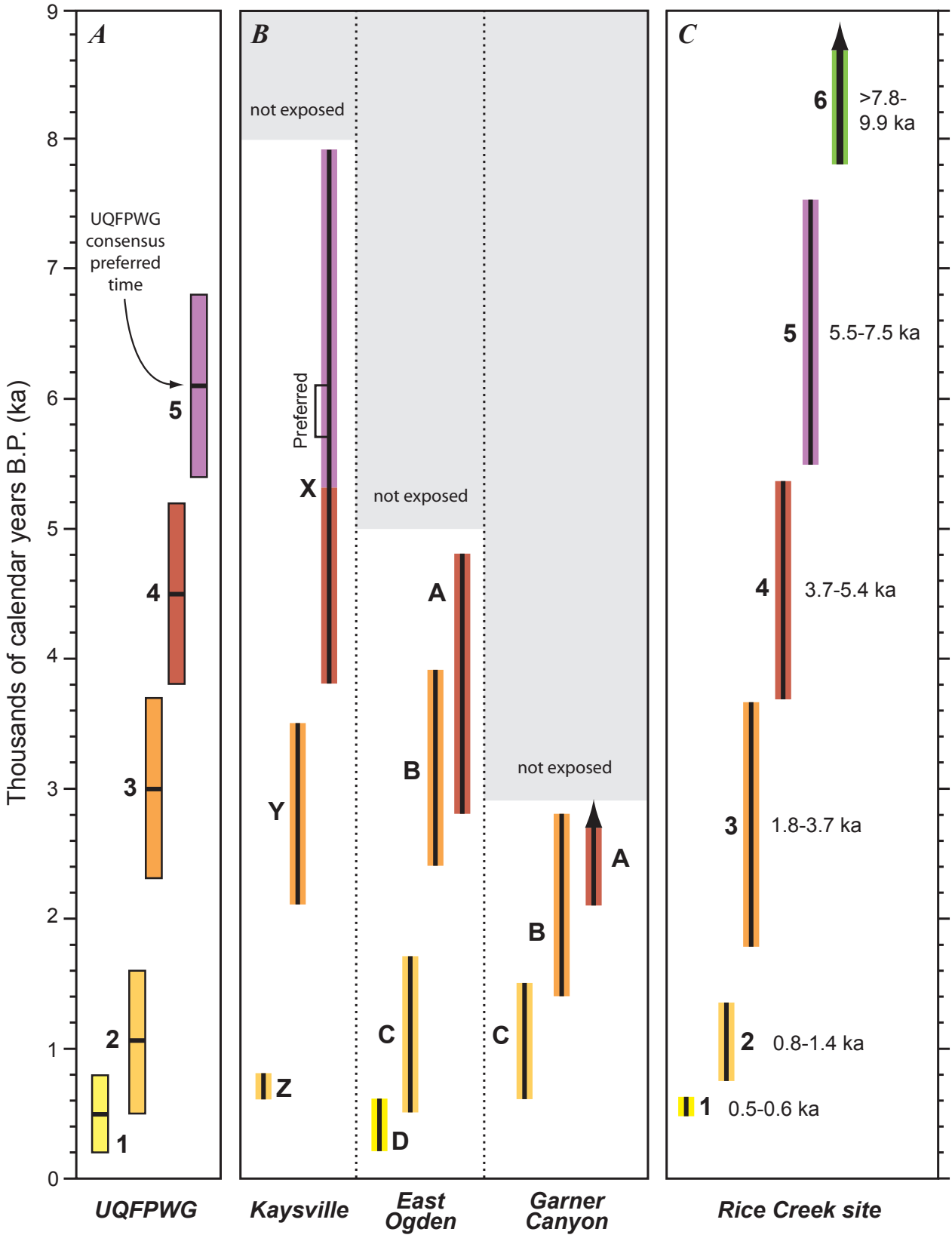

Figure 11. *Comparison of earthquake-timing data for the Weber segment, showing (A) consensus time ranges (colored boxes) of the Utah Quaternary Fault Parameters Working Group (UQFPWG; Lund, 2005); (B) paleoseismic timing data from the Kaysville, East Ogden, and Garner Canyon sites (table 1); and (C) the Rice Creek paleoearthquake chronology. The dual-colored third event (X) at Kaysville represents uncertainty in whether this event is Weber-segment earthquake 4 or 5. All data are cal yr B.P.*

displacement of >0.6–0.7 m), which is consistent with existing Weber-segment per-event displacement data that average 2.1 ± 1.3 m (DuRoss, 2008). The average Holocene slip rate at the Rice Creek site (0.9–2.1 mm/yr) is consistent with the Nelson and others (2006) estimate of 1–2 mm/yr, based on paleoseismic displacement data and scarp-profile data for the segment; the McCalpin and others (1994) estimate of 0.7–1.7 mm/yr, based on displacement in Kaysville earthquakes; and a longer-term (latest Pleistocene to present) slip rate of 1.6 mm/yr, based on displaced Lake Bonneville deposits (Nelson and Personius, 1993). The UQFPWG (Lund, 2005) consensus slip rate is 0.6–1.2–4.3 mm/yr.

CONCLUSIONS

Stratigraphic and structural evidence in two fault trenches, radiocarbon and luminescence ages, and results of OxCal modeling indicate that at least five, and probably six, earthquakes occurred on the northern Weber segment in the past 8–10 kyr. Per-event displacements for these earthquakes are large, averaging 1.6–2.5 m. Recurrence intervals average 1500 yr (two-sigma range of 500–3100 yr), and using total displacement, the average vertical slip rate for the site is 0.9–2.1mm/yr. These estimates are consistent with previous investigations as well as the consensus of the UQFPWG (Lund, 2005). The Rice Creek paleoseismic data include a previously unknown sixth earthquake, which extends the Weber-segment paleoseismic record into the early Holocene. We also documented a ~500-yr most-recent earthquake. We correlate the ~500-yr Rice Creek earthquake with the ~500-yr East Ogden earthquake, which together provide evidence for a partial rupture of the northern Weber segment.

ACKNOWLEDGMENTS

This work was supported by the U.S. Geological Survey National Earthquake Hazards Reduction Program (award no. 07HQGR0093) and the Utah Geological Survey. The USDA Forest Service (Chip Sibbernsen and Rick Vallejo from the Ogden District) and private landowner J. Dee Curtis granted land access. We thank Stephanie Davi (Utah State University); Michael Machette and Alan Nelson (USGS); and Bill Lund, Tyler Knudsen, and Ashley Elliot (UGS) for their assistance in the field and discussions of this work. Reviews by Alan Nelson (USGS) and William Lund, Steve Bowman, and Michael Hylland (UGS) strengthened this report.

REFERENCES

Aitken, M.J., 1994, Optical dating—a non-specialist review: Quaternary Geochronology (Quaternary Science Reviews), v. 13, p. 503–508.

Bennett, R.A., Wernicke, B.P., Niemi, N.A., Friedrich, A.M., and Davis, J.L., 2003, Contemporary strain rates in the northern Basin and Range Province from GPS data: Tectonics, v. 22, no. 2, 29 p.

Black, B.D., Hecker, S., Hylland, M.D., Christenson, G.E., and McDonald, G.N., 2003, Quaternary fault and fold database and map of Utah: Utah Geological Survey Map 193DM, scale 1:50,000, compact disk.

Bronk Ramsey, C., 1995, Radiocarbon calibration and analysis of stratigraphy—the OxCal program: Radiocarbon, v. 37, no. 2, p. 425–430.

Bronk Ramsey, C., 2001, Development of the radiocarbon program OxCal: Radiocarbon, v. 43, no. 2a, p. 355–363.

Bronk Ramsey, C., 2008, Depositional models for chronological records: Quaternary Science Reviews, v. 27, no. 1-2, p. 42–60.

Chang, W.L., and Smith, R.B., 2002, Integrated seismic-hazard analysis of the Wasatch Front, Utah: Bulletin of the Seismological Society of America, v. 92, no. 5, p. 1904–1922.

Chang, W.L., Smith, R.B., Meertens, C.M., and Harris, R.B., 2006, Contemporary deformation of the Wasatch fault, Utah, from GPS measurements with implications for interseismic fault behavior and earthquake hazard—observations and kinematic analysis: Journal of Geophysical Research, vol. 111, 19 p.

Cluff, L.S., Brogan, G.E., and Glass, C.E., 1970, Wasatch fault, northern portion—earthquake fault investigation and evaluation, a guide to land-use planning: Oakland, California, Woodward-Clyde and Associates, variously paginated.

DuRoss, C.B., 2008, Holocene vertical displacement on the central segments of the Wasatch fault zone, Utah: Bulletin of the Seismological Society of America, v. 98, no. 6, p. 2918–2933.

Forman, S.L., Nelson, A.R., and McCalpin, J.P., 1991, Thermoluminescence dating of fault-scarp-derived colluvium—deciphering the timing of earthquakes on the Weber segment of the Wasatch fault zone, north-central Utah: Journal of Geophysical Research, v. 96, no. B1, p. 595–605.

Godsey, H.S., Currey, D.R., and Chan, M.A., 2005, New evidence for an extended occupation of the Provo shoreline and implications for regional climate change, Pleistocene Lake Bonneville, Utah, USA: Quaternary Research, v. 63, no. 2, p. 212–223.

Huntley, D.J., Godfrey-Smith, D.I., and Thewalt, M.L.W., 1985, Optical dating of sediments: Nature, v. 313, p. 105–107.

Lund, W.R., 2005, Consensus preferred recurrence-interval and vertical slip-rate estimates—review of Utah paleoseismic-trenching data by the Utah Quaternary Fault Parameters Working Group: Utah Geological Survey Bulletin 134, compact disk.

Machette, M.N., Personius, S.F., and Nelson, A.R., 1992, Paleoseismology of the Wasatch fault zone—a summary of recent investigations, interpretations, and conclusions, *in* Gori, P.L., and Hays, W.W., editors, Assessment of regional earthquake hazards and risk along the Wasatch Front, Utah: U.S. Geological Survey Professional Paper 1500-A, p. A1–A71.

Matthews, M.H., 1979, Soil sample analysis of 5MT2148—Dominguez Ruin, Dolores, Colorado, *in* Reed, A.D., editor, The Dominguez Ruin—a McElmo Phase pueblo in southwestern Colorado: Bureau of Land Management Cultural Resource Series, v. 7, variously paginated.

Martinez, L.J., Meertens, M., and Smith, R.B., 1998, Rapid deformation rates along the Wasatch fault zone, Utah, from first GPS measurements with implications for earthquake hazard: Geophysical Research Letters, v. 25, no. 4, p. 567–570.

McCalpin, J.P., 1996, Paleoseismology in extensional tectonic environments, *in* McCalpin, J.P., editor, Paleoseismology: San Diego, Academic Press, 588 p.

McCalpin, J.P., 2002, Paleoseismology of Utah, Volume 10—Post-Bonneville earthquake chronology of the Salt Lake City segment, Wasatch fault zone, from the 1999 "Megatrench" site: Utah Geological Survey Miscellaneous Publication 02-7, 37 p.

McCalpin, J.P., and Forman, S.L., 2002, Paleoseismology of Utah, Volume 11—Post-Provo earthquake chronology of the Brigham City segment, Wasatch fault zone, Utah: Utah Geological Survey Miscellaneous Publication 02-9, 46 p.

McCalpin, J.P., Forman, S.L., and Lowe, M., 1994, Reevaluation of Holocene faulting at the Kaysville site, Weber segment of the Wasatch fault zone, Utah: Tectonics, v. 13, no. 1, p. 1–16.

McCalpin, J.P., and Nishenko, S.P., 1996, Holocene paleoseismicity, temporal clustering, and probabilities of future large (M>7) earthquakes on the Wasatch fault zone: Journal of Geophysical Research, v. 101, no. B3, p. 6233–6253.

National Aeronautics & Space Administration (NASA), 2006, Visible Earth—a catalog of NASA images and anima-

tions of our home planet: Online, <http://visibleearth.nasa.gov/>, accessed July 2006.

Nelson, A.R., 1988, The northern part of the Weber segment of the Wasatch fault zone near Ogden, Utah, *in* Machette, M.N., editor, In the footsteps of G.K. Gilbert—Lake Bonneville and neotectonics of the eastern Basin and Range Province, Guidebook for Field Trip Twelve: Utah Geological and Mineral Survey Miscellaneous Publication 88-1, p. 33–37.

Nelson, A.R., 1992, Lithofacies analysis of colluvial sediments—an aid in interpreting the recent history of Quaternary normal faults in the Basin and Range Province, western United States: Journal of Sedimentary Petrology, v. 62, p. 607–621.

Nelson, A.R., Klauk, R.H., Lowe, M., and Garr, J.D., 1987, Holocene history of displacement on the Weber segment of the Wasatch fault zone at Ogden, northern Utah [abs.]: Geological Society of America Abstracts with Programs, v. 19, no. 5, p. 322.

Nelson, A.R., Lowe, M., Personius, S., Bradley, L.A., Forman, S.L., Klauk, R., and Garr, J., 2006, Paleoseismology of Utah, Volume 13—Holocene earthquake history of the northern Weber segment of the Wasatch fault zone, Utah: Utah Geological Survey Miscellaneous Publication 05-8, 39 p., 2 plates.

Nelson, A.R., and Personius, S.F., 1993, Surficial geologic map of the Weber segment, Wasatch fault zone, Weber and Davis Counties, Utah: U.S. Geological Survey Miscellaneous Investigations Series Map I-2199, 22 p. pamphlet, scale 1:50,000.

Olig, S., McDonald, G., Black, B., DuRoss, C., and Lund, B., 2004, The Mapleton "megatrench," deciphering 11,000 years of earthquake history on the Wasatch fault near Provo: Utah Geological Survey, Survey Notes, v. 32, no. 2, p. 4–6.

Oviatt, C.G., 1997, Lake Bonneville fluctuations and global climate change: Geology, v. 25, p. 155–158.

Prescott, J.R., and Hutton, J.T., 1994, Cosmic ray contributions to dose rates for luminescence and ESR dating: Radiation Measurements, v. 23, p. 497–500.

Puseman, K., and Cummings, L.S., 2005, Separation and identification of charcoal and organics from bulk sediment samples for improved radiocarbon dating and stratigraphic correlations, *in* Lund, W.R., editor, Western States Seismic Policy Council Proceedings Volume of the Basin and Range Province Seismic Hazards Summit II: Utah Geological Survey Miscellaneous Publication 05-2, 10 p., compact disk.

Reimer, P.J., Baillie, M.G.L., Bard, E., Bayliss, A., Beck, J.W., Bertrand, C., Blackwell, P.G., Buck, C.E., Burr, G., Cutler, K.B., Damon, P.E., Edwards, R.L., Fairbanks, R.G., Friedrich, M., Guilderson, T.P., Hughen, K.A., Kromer, B., McCormac, F.G., Manning, S., Bronk Ramsey, C., Reimer, R.W., Remmele, S., Southon, J.R., Stuiver, M., Talamo, S., Taylor, F.W., van der Plicht, J., and Weyhenmeyer, C.E., 2004, IntCal04 terrestrial radiocarbon age calibration, 0-26 cal kyr BP: Radiocarbon, v. 46, no. 3, p. 1029–1058.

Schwartz, D.P., and Coppersmith, K.J., 1984, Fault behavior and characteristic earthquakes—examples from the Wasatch and San Andreas fault zones: Journal of Geophysical Research, v. 89, p. 5681–5698.

Swan, F.H., III, Schwartz, D.P., and Cluff, L.S., 1980, Recurrence of moderate to large magnitude earthquakes produced by surface faulting on the Wasatch fault zone, Utah: Bulletin of the Seismological Society of America, v. 70, p. 1431–1462.

Swan, F.H., III, Schwartz, D.P., Hanson, K.L., Knuepfer, P.L., and Cluff, L.S., 1981, Study of earthquake recurrence intervals on the Wasatch fault at the Kaysville site, Utah: U.S. Geological Survey Open-File Report 81-228, 30 p.

U.S. Department of Agriculture, 1993, Soil Survey Manual: Online, <http://soils.usda.gov/technical/manual/>, accessed April 2009.

U.S. Department of Agriculture, 2008, Aerial photography field office—National Agriculture Imagery Program: Online, <http://165.221.201.14/ NAIP.html>, accessed August 2008.

U.S. Geological Survey, 2008, United States National Seismic Hazard Maps: Online, <http://earthquake.usgs.gov/research/hazmaps/>, accessed July 2008.

Yonkee, A., and Lowe, M., 2004, Geologic map of the Ogden 7.5-minute quadrangle, Weber and Davis Counties, Utah: Utah Geological Survey Map 200, 42 p., scale 1:24,000, 2 plates.

APPENDICES

APPENDIX A

DESCRIPTION OF STRATIGRAPHIC UNITS IN TRENCHES AT THE RICE CREEK SITE

Unit[1]	Matrix texture[2]	% matrix/ gravel[3]	Clasts: %<2mm/2 mm-1cm/1-3cm/>3cm	Clasts: Largest/ avg size (cm)	Clast or matrix support	Sorting	Bedding	Color[4] dry (moist)	Consistence[5]: Dry	Consistence[5]: Wet	Lower bound[6]	Soil development[7]	Genesis
Footwall of upper fault zone													
Soil on unit 4c (S4)	sandy loam	30/70	30/20/30/20	10/1-2	matrix	poor	massive; aligned clasts	*7.5YR4/2 (5YR2.5/2)*	sh	ss/po	a	A horizon; massive; no structure	NA
4c	sand	15/85	15/40/30/15	25-35/8-10	variable	fair	massive to mod. stratified; locally mod. well bedded	*10YR7/3 (10YR6/3)*	so	so/po	ne	none	alluvial-fan gravels
Hanging wall of upper fault zone; footwall of lower fault zone (includes north-wall exposure of main trench)													
1a	loamy sand	25/75	25/35/20/20	15/2-4	matrix	poor	massive	*10YR4/2 (10YR2/2)*	so	so/po	g/s	none	wash-facies colluvium
1b	loamy sand	40/60	40/30/20/10	10-12/1-3	variable	poor	massive to weakly stratified	*10YR4.5/3 (10YR3/3)*	lo	so/po	a/w	locally contains soil blocks	debris-facies colluvium
2a (west)	loamy sand	40/60	25/25/25/25	12/1-2	matrix	fair	massive to weakly stratified; clasts aligned with unit base	*10YR4/2 (10YR3/2)*	so	so/po	g/w	none	wash-facies colluvium
2a (east)	loamy sand	30/70	30/25/25/20	10-15/2-5	matrix	poor	massive; slope parallel clasts	*10YR5.5/6 (10YR4/4)*	sh	so/po	c/w	capped by modern slope wash	wash-facies colluvium
2b (west)	loamy sand	10/90	10/15/15/60	20-25/4-7	clast	poor	massive to weakly stratified in downslope direction	*10YR5/4 (10YR4.5/4)*	lo	so/po	a/s	none	debris-facies colluvium
2b (east)	loamy sand	30/70	30/30/20/20	8-10/2-5	variable	poor	massive	*10YR6/4 (10YR4/5)*	so	so/po	c/s	none	debris-facies colluvium
Soil on unit 3 (S3)	loamy sand	20/80	20/25/25/30	27/4-8	matrix	poor	massive	*10YR7/4 (10YR4/4)*	so-sh	so/po	a/s	none	wash-facies colluvium
3a	silty sand-sand	25/75	25/25/25/25	7-10/2-4	variable	poor	massive to weakly stratified; clasts aligned downslope	*10YR8/4 (10YR6/4)*	lo-so	so/po	a/s	none	wash-facies colluvium
3b	loamy sand	30/70	30/30/10/30	30/6-10	matrix	poor	massive	*10YR8/4 (10YR5.5/6*	so	so/po	a-c/s-w	none	debris-facies colluvium
4s	sand	20/80	20/30/25/25	15-20/2-5	clast (sand)	good	NA (sheared); clasts locally aligned parallel to fault planes	*10YR8/3 (10YR7/7)*	lo	so/po	NA	none	sheared sediment
4b	silty sand-loamy sand	25/75	25/25/25/25	30-35/4-8	mostly clast	poor to fair	massive to weakly bedded	*10YR 8/3 (10YR5/6)*	so-sh	so/po	ne	30-35 cm A horizon minor oxidation	alluvial-fan gravels
4b-df	loamy sand	40/60	40/1/1/58	30/4-8	matrix	poor; bimodal	massive	*10YR7/4 (10YR5/6)*	so	so/po	a/w	40-45 cm at sample site	debris flow
4b-sd	sand	>99/<1	99/<1/<1/<1	m-f sand	clast (sand)	good	massive to weakly laminated	*10YR7/3 (10YR6/6)*	so	so/po	a	none	sand lense in alluvial-fan deposits

Unit[1]	Matrix texture[2]	% matrix/ gravel[3]	Clasts		Clast or matrix support	Sorting	Bedding	Color[4] dry (moist)	Consistence[5]		Lower bound[6]	Soil development[7]	Genesis
			%<2mm/2 mm-1cm/1-3cm/>3cm	Largest/ avg size (cm)					Dry	Wet			
Hanging wall of lower fault zone													
1a	gravelly silt	60/40	60/20/15/5	12/1-2	matrix	poor	massive to weakly stratified; slope parallel clasts	*10YR5/3.5 (10YR3/3)*	sh	so/ps	a/s	A horizon; massive, no structure	wash-facies colluvium
1b (east)	sandy silt	50/50	50/20/20/10	10/1-3	mostly clast	poor-fair	massive	*10YR6/6 (10YR5/6)*	lo	so/po	c/w	none	debris-facies colluvium
1b (east)1	silty sand	60/40	60/10/20/10	13/2-4	matrix	poor	massive to weakly stratified; slope parallel clasts	*10YR5/2 (10YR3/3)*	sh	ss/ps	a/s-w	15-cm thick organic-rich zone	wash-facies colluvium
1b (east)2	silty sand	55/45	55/5/20/20	20/1-3	matrix	poor	massive	*10YR5/4 (10YR4/4)*	lo-sh	ss/ps	a/w	minor soil organics	debris-facies colluvium
2a	silty sand	60/40	60/25/10/5	9/0.5-1	matrix	poor	massive with weakly stratified gravel lenses	*10/YR4/3 (10YR3/3)*	sh	s/p	c/w	weak 10-15-cm thick A horizon	wash-facies colluvium
2b	sandy silt	75/25	50/10/25/15	6/1-3	mostly matrix	poor-mod.	massive with weakly stratified gravel lenses	*10YR4/3 (10YR2/2)*	sh	s/p	c/w-i	organics-rich matrix	debris-facies colluvium
4s	silty sand	50/50	50/15/20/15	17/1-3	clast	poor	NA (sheared); clasts locally aligned parallel to fault planes	*10YR6/4 (10YR5/4)*	lo	so/po	a/s-w	none	sheared sediment
soil on unit 3 (S3)	sandy loam	75/25	75/15/5/5	6/0.5-1	matirx	poor	massive	*10/YR4/4 (10YR3/3)*	sh	so/ps	g/w-i	buried soil organics on unit 3; no structure	NA
4a	silty sand	30/70	30/30/20/20	24/2-4	mostly clast	poor to mod.	massive to moderately stratified	*10YR8/4 (10YR6/6)*	lo-sh	so/po	a-c/s-w	25-30-cm thick A horizon at surface	alluvial-fan gravels
4a-df	silty sand	70/30	70/<5/15/20	15/2-5	matrix	poor; bimodal	massive	*10YR6/4 (10YR4/4)*	so	ss/ps	c/s-w	weak A horizon	debris flow
4a-sd	sand	75/25	75/20/10/5	10/0.5-1	clast (sand)	good	massive to weakly laminated	*10YR7/4 (10YR6/6)*	lo	so/po	a/s-w	none	sand lense in alluvial-fan deposits
Antithetic fault zone (hangingwall of lower fault zone; includes north-wall exposure)													
1a	sandy silt	60/40	60/20/10/10	7/1-2	matrix	poor	massive with weakly stratified gravel lenses	*10YR3/3.5(10YR2/2)*	lo-so	ss/p	c/w	organic-rich A horizon	wash-facies colluvium
1b	sandy silt	55/45	55/25/15/5	14/1-2	matrix	poor	massive	*10YR5/3 (10YR3/3)*	so	ss/ps-p	c/w	organics-rich matrix	debris-facies colluvium
soil on unit 2 (S2)	sandy silt	65/35	65/25/10/<1	10/0.5-1	matrix	poor	massive	*10YR4/4 (10YR3/2)*	sh	so/ps	g/w-i	soil organics on unit 2	NA
2	sandy silt	55/45	55/20/15/10	7/1-3	matrix	poor	massive with weakly stratified gravel lenses	*10YR5/3 (10YR3/3)*	sh	ss/ps	c-g/w	locally organics-rich matrix	undivided scarp colluvium
3a	silty sand	65/35	65/20/5/10	21/0.5-2	mostly clast	poor-mod.	massive to weakly stratified	*10YR8/4 (10YR6/4)*	lo-sh	so/po	c-g/s-w	25-30-cm thick A horizon; 12-cm silt cap	alluvial-fan gravels

Unit[1]	Matrix texture[2]	% matrix/ gravel[3]	Clasts		Clast or matrix support	Sorting	Bedding	Color[4] dry (moist)	Consistence[5]		Lower bound[6]	Soil development[7]	Genesis
			%<2mm/2 mm-1cm/1-3cm/>3cm	Largest/ avg size (cm)					Dry	Wet			
Soil description (horizontal meter-mark 70.5)[8]													
A (20 cm)	loam	40/60	-	-	-	-	-	*10YR4/2(10YR 3/2)*	sh	ss/ps	a/w	A horizon; grade: 1; size, shape: vf, gr	-
AB (37 cm)	sandy loam	50/50	-	-	-	-	-	*7.5YR5/4 (7.5YR4/3)*	so	so/po	c/w	AB horizon; grade: sg; size, shape: vf, gr	-
COX (62 cm)	loamy sand	60/40	-	-	-	-	-	*10YR6/3 (10YR4/6)*	lo-so	so/po	a/s	COX horizon; grade: m; size, shape: NA	-
2COX2 (79 cm)	sand	40/60	-	-	-	-	-	*10YR6/3 (10YR4/4)*	lo	so/po	c/s	2COX2 horizon; grade: m; size, shape: NA	-
Cu (ne)	sand	40/60	-	-	-	-	-	*10YR8/4 (10YR5/4)*	lo	so/po	-	Cu horizon; grade: m; size, shape: NA	-

[1] Units as shown on plate 1. For soil description (last five rows), units are soil horizons with basal depths in parentheses (ne, base not exposed).

[2] Texture terms follow the U.S. Department of Agriculture (1993) classification system. Textural information may not be representative of entire unit due to vertical and horizontal heterogeneity in units.

[3] Percentages of clast-size fractions (based on area) are field estimates. We used a #10 (2 mm) sieve to separate matrix from gravel.

[4] Munsell color of matrix.

[5] Dry consistence: lo – loose, so – soft, sh – slightly hard, h – hard. Wet consistence: so – nonsticky, ss – slightly sticky, s – sticky; po – nonplastic, ps – slightly plastic, p – plastic.

[6] Lower boundary. Distinctness: a – abrupt (1mm-2.5 cm), c – clear (2.5-6 cm), g – gradual (6-12.5 cm). Topography: s – smooth, w – wavy, i – irregular. ne, base of unit not exposed.

[7] Description of soil development, including soil-structure information (under soil description subheading). Grade: 1 - weak, sg - single grain, m - massive; size: vf - very fine; shape: gr - granular. No clay films were observed. NA – not applicable.

[8] Described by Stephen Personius; see plate 1 for location.

APPENDIX B

SUMMARY OF ^{14}C-DATED CHARCOAL CONCENTRATED FROM BULK SEDIMENT SAMPLES FROM THE RICE CREEK SITE

Sample number	Station (m)[1]	Depth (m)	Unit sampled	Material sampled[2]	Organic material dated (weight in mg)[3]	Pre-treatment method[4]	Relation to earthquake[5]	Acc. No.[6]	Age (^{14}C yr B.P.)[7]	d^{13}C[8]	Age range (cal yr B.P.)[9]
Upper fault zone											
C5	22.5, 23.7^{N}	0.72	Base of 1a	Colluvium	8 frag. Asteraceae charcoal (5)	ABA	Min – U1	64256	130 ± 75	-27.38	0-294
C2	23.5, 24.7	0.52	Base of unit 1a	Colluvium	6 frag. unidentified charcoal (1)	A	Min – U1	65815	1630 ± 40	-25.39	1400-1690
C6	22.5, 23.7^{N}	0.82	Top of unit 2a	A horizon?	3 frag. Asteraceae charcoal (1)	A	Max – U1	63558	1650 ± 35	-23.89	1420-1700
C1a	23.1, 24.6	0.58	Top of unit 2a	A horizon?	5 frag. Asteraceae charcoal (7)	ABA	Max – U1	64284	2390 ± 25	-24.13	2340-2680
C1b	23.1, 24.6	0.58	Top of unit 2a	A horizon?	2 frag. *Quercus*; 9 frag. unidentified charcoal (1)	A	Max – U1	65839	835 ± 30	-24.55	670-810
C7	21.6, 23.7^{N}	1.04	Unit 2a	Colluvium (organic-rich lens)	2 frag. *Opuntia* (genus cacti) seed (2)	ABA	Min – U2	65818	>modern	-14.74	>modern
C8	21.6, 23.5^{N}	1.50	Unit 2b	A horizon (soil block in colluvium)	34 frag. unidentified charcoal (2)	ABA	Max – U2	65813	1440 ± 40	-24.75	1270-1410
C4a	24.0, 23.6	1.24	Top of unit 3	A horizon	4 frag. *Juniperus* charcoal (5)	ABA	Max – U2[a]	63559	4730 ± 45	-22.59	5320-5590
C4b	24.0, 23.6	1.24	Top of unit 3	A horizon	Numerous frag. unidentified charcoal (4)	ABA	Max – U2[a]	66055	4770 ± 50	-23.23	5320-5600
C3a	23.3, 23.1	1.04	Top of unit 3	A horizon	8 frag. *Juniperus* charcoal (2)	ABA	Max – U2[a]	63555	4750 ± 40	-22.3	5320-5590
C3b	23.3, 23.1	1.04	Top of unit 3	A horizon	57 frag. unidentified charcoal (4)	ABA	Max – U2	66125	4210 ± 80	-24.54	4520-4970
Lower fault zone											
C9	51.6, 15.0	0.44	Base of unit 1a	Colluvium (organic-rich lens)	34 frag. unidentified charcoal (2)	ABA	Min – L1	65822	460 ± 30	-24.75	470-540
C11	54.1, 13.7	0.46	Top of unit 1b	Colluvium	20 frag. dicot charcoal (11)	ABA	Min – L1	63764	105 ± 35	-25.11	10-270
C10	52.2, 14.6	0.64	Top of unit 1b	Colluvium	6 frag. unidentified charcoal (<1)	A	-	66126	3690 ± 70	-25.16	3840-4240
C12	54.4, 13.6	0.50	Top of unit 1b	Colluvium	56 frag. unidentified charcoal (5)	ABA	Min – L1?	63768	560 ± 40	-25.9	510-650
C14a	55.6, 13.3	0.40	Base of unit 1a	Colluvium	4 frag. *Artemisia* charcoal (3)	ABA	-	63573	>modern	-27.48	>modern
C14b	55.6, 13.3	0.40	Base of unit 1a	Colluvium	13 frag. dicot charcoal (2)	ABA	-	63556	>modern	-26.23	>modern
C13	54.6, 13.3	0.78	Top of unit 2a	A horizon?	4 frag. Asteraceae charcoal (3)	ABA	Max – L1?	63761	560 ± 35	-25.7	510-650
C20	52.5, 14.2	0.80	Top of unit 2b	A horizon?	9 frag. unidentified charcoal (1)	A	-	64234	115 ± 60	-27.05	20-290
C15	56.3, 12.6	0.86	Soil on unit 4a-1	A horizon	29 frag. unidentified charcoal (2)	ABA	Max – L2	63561	3430 ± 35	-23.67	3580-3830
C18	59.1, 11.8	0.74	Base of unit 2	Colluvium	2 frag. Asteraceae; 11 frag. dicot charcoal (1)	A	Min – L2	64241	835 ± 85	-25.75	640-930
C19	59.1, 11.8	0.80	Top of unit 4a-1	A horizon	10 frag. unidentified charcoal (1)	A	Max – L2	64243	1830 ± 65	-25[a]	1590-1930
C16	58.2, 12.3	0.46	Base of unit 1	Colluvium	7 frag. Asteraceae and 4 frag. dicot charcoal (1)	A	-	65903	>modern	-26.35	>modern
C17	58.2, 12.1	0.62	Unit 2	Colluvium	46 frag. unidentified charcoal (2)	ABA	Max – L2	65819	700 ± 35	-25.7	540-720
Antithetic fault zone											
C22	93.3, 5.6	0.46	Base of unit 1a	Colluvium (organic-rich lens)	No dateable material	-	-	-	-	-	-
C21	92.9, 5.4	0.66	Top of unit 2	A horizon	4 frag. Asteraceae charcoal (<1)	A	Max – AL1	65823	2900 ± 35	-24.79	2930-3180
C23	92.5, 5.5	0.66	Top of unit 2	A horizon	No dateable material	-	-	-	-	-	-
C24	94.2, 5.7	0.38	Top of unit 2	A horizon	No dateable material	-	-	-	-	-	-

[1] Station coordinates are horizontal and vertical meter marks along arbitrary reference grid for the site (plate 1). ^{N} indicates station coordinates for the north wall of the main trench.
[2] Colluvium indicates the organic-rich sediment (matrix) of scarp colluvium, including organic-rich lenses; A horizon indicates organic-rich A-horizon sediment.
[3] Separation and identification by Paleo Research Institute (Golden, Colorado). Dicot indicates Monocot/Herbaceous dicot.
[4] ABA – acid-base-acid wash, A – acid-wash only.
[5] Max (or min) indicates sample provides a maximum- (or minimum-) limiting time constraint for a surface-faulting earthquake (e.g., U1). [a]Samples C4 and C5 also provide minimum-limiting constraints for earthquake U3.
[6] Accession number from the National Ocean Sciences Accelerator Mass Spectrometry Facility (NOSAMS) at the Woods Hole Oceanographic Institution.
[7] Laboratory-reported ^{14}C age with one standard-deviation uncertainty. B.P. is before present (1950).
[8] Delta ^{13}C value, measured by NOSAMS; [a] indicates an assumed value.
[9] Two-sigma, calendar-calibrated age ranges rounded to nearest decade and determined using OxCal calibration software (v. 4.0, Bronk Ramsey, 1995, 2001) and the IntCal 2004 atmospheric data set (Reimer and others, 2004).

APPENDIX C
QUARTZ BLUE-LIGHT OPTICALLY STIMULATED LUMINESCENCE AGES FOR THE RICE CREEK SITE

Sample information[1]	Water content (%)[2]	Potassium (%)[3]	Thorium (ppm)[3]	Uranium (ppm)[3]	Cosmic dose additions (Gy/kyr)[4]	Total dose rate (Gy/kyr)	Equivalent dose (Gy)	Aliquots[5]	Age (ka)[6]	Two-sigma age range (ka)
L1	7 (33)	2.13 ± 0.10	12.0 ± 0.29	3.23 ± 0.11	0.20 ± 0.01	3.47 ± 0.06	23.9 ± 3.63	15 (30)	6.87 ± 1.05[a]	4.8-9.0
L2	4	1.51	7.9	1.5	0.25	2.28 ± 0.11	20.06 ± 7.53	31(73)	8.79 ± 3.34[b]	2.1-15.5
L3	4 (14)	1.08 ± 0.05	6.07 ± 0.19	1.56 ± 0.08	0.21 ± 0.01	2.04 ± 0.04	28.8 ± 3.46	18 (30)	14.1 ± 1.72	10.7-17.5
L4	18 (48)	1.48 ± 0.04	7.67 ± 0.21	2.09 ± 0.08	0.21 ± 0.01	2.20 ± 0.04	33.2 ± 3.04	17 (40)	13.9 ± 1.13	11.6-16.2
L5	1 (48)	1.14 ± 0.08	6.26 ± 0.17	1.74 ± 0.07	0.22 ± 0.01	1.81 ± 0.04	2.76 ± 0.59	16 (35)	1.52 ± 0.33	0.9-2.2
L6	1 (49)	1.25 ± 0.09	7.06 ± 0.19	2.02 ± 0.08	0.23 ± 0.01	2.00 ± 0.05	17.8 ± 0.99	17 (50)	8.87 ± 0.53	7.8-9.9

[1] Samples obtained using opaque PVC tubes. Sample L2 analyzed by the Utah State University luminescence laboratory, all other samples analyzed by the U.S. Geological Survey.

[2] Field moisture; complete sample saturation percent in parentheses. Ages calculated using 35-50% of saturation values.

[3] Analyses obtained using laboratory gamma spectrometry (low-resolution NaI detector) and *in situ* gamma spectrometry.

[4] Cosmic doses and attenuation with depth were calculated using the methods of Prescott and Hutton (1994); Gy – gray.

[5] Number of accepted aliquots; total number of analyses in parentheses.

[6] Equivalent dose and age for fine-grained 125-250 μm quartz sand ([a]90-105 μm quartz sand for sample L1; [b]63-250 μm quartz sand for sample L2). Linear + exponential fit used on age, errors to one standard deviation.

APPENDIX D

OXCAL MODELS

OxCal models for the Rice Creek site were created using OxCal calibration and analysis software (version 4.0; Bronk Ramsey, 1995, 2001, 2008; using the IntCal04 calibration curve of Reimer and others, 2004). The models include *C_Date* for luminescence ages, *R_Date* for radiocarbon ages, and Date for undated events (paleoearthquakes). These components are arranged into ordered sequences based on the relative stratigraphic positions of the samples. The sequences may contain *phases*, or groups where the relative stratigraphic ordering information for the individual radiocarbon ages is unknown. The *Difference* command computes two-sigma recurrence intervals between the paleoearthquakes. The models are presented here in reverse stratigraphic order, following the order in which the ages and events are evaluated in OxCal (e.g., earthquake 5 occurs before 4).

Models A and B (Upper Fault Zone)

OxCal models A and B are identical, with the exception that radiocarbon age C1b is used only in model A (shown below). Radiocarbon ages C3a, C3b, C4a, and C4b are included in both models, but a variation to the model excludes C3b (see OxCal Modeling section in main text for discussion).

```
Sequence("Rice Creek model A")
{
 Boundary("start");
 C_Date("L6, 8870+/-530", -6870, 530);
 C_Date("L1, 6870+/-1050", -4870, 1050);
 Date("Earthquake U3");
 Phase("A horizon on U3 colluvium")
 {
  R_Date("C3a, 4750+/-40", 4750, 40);
  R_Date("C3b, 4210+/-80", 4210, 80); [This age excluded in model D]
  R_Date("C4a, 4730+/-45", 4730, 45);
  R_Date("C4b, 4770+/-50", 4770, 50);
 };
 Date("Earthquake U2");
 Phase("U2 colluvium")
 {
  R_Date("C1a, 2390+/-25", 2390, 25);
  R_Date("C6, 1650+/-35", 1650, 35);
  R_Date("C8, 1440+/-40", 1440, 40);
  R_Date("C1b, 835+/-30", 835, 30); [This age excluded in models B and D]
 };
 Date("Earthquake U1");
 R_Date("C5, 130+/-75", 130, 75);
 C_Date("Historical constraint", 1850 AD, 0);
 Boundary("end");
};
```

Model C (Lower Fault Zone)

OxCal model C excludes samples C10, C12, and C20 (see Correlation of Earthquakes section in main text for discussion).

```
Sequence("Rice Creek model C")
{
 Boundary("start");
 R_Date("C15, 3430+/-35", 3430, 35);
 Date("Earthquake L3");
 R_Date("C19, 1830+/-65", 1830, 65);
```

```
 Date("Earthquake L2");
 R_Date("C18, 835+/-85", 835, 85);
 R_Date("C17, 700+/-35", 700, 35);
 R_Date("C13, 560+/-35", 560, 35);
 Date("Earthquake L1");
 Phase("L1 colluvium")
 {
  R_Date("C9, 460+/-30", 460, 30);
  R_Date("C11, 105+/-35", 105, 35);
 };
 C_Date("Historical constraint", 1850 AD, 0);
 Boundary("end");
};
```

Model D (Entire Site)

```
Sequence("Rice Creek model D")
{
 Boundary("start");
 C_Date("L6, 8870+/-530", -6870, 530);
 C_Date("L1, 6870+/-1050", -4870, 1050);
 Date("Earthquake 5");
 Phase("A horizon on U3 colluvium")
 {
  R_Date("C3a, 4750+/-40", 4750, 40);
  R_Date("C4a, 4730+/-45", 4730, 45);
  R_Date("C4b, 4770+/-50", 4770, 50);
 };
 Date("Earthquake 4");
 R_Date("C15, 3430+/-35", 3430, 35);
 Date("Earthquake 3");
 Phase("U2 colluvium")
 {
  R_Date("C19, 1830+/-65", 1830, 65);
  R_Date("C6, 1650+/-35", 1650, 35);
  R_Date("C8, 1440+/-40", 1440, 40);
 };
 Date("Earthquake 2");
 R_Date("C18, 835+/-85", 835, 85);
 R_Date("C17, 700+/-35", 700, 35);
 R_Date("C13, 560+/-35", 560, 35);
 Date("Earthquake 1");
 Phase("L1 colluvium")
 {
  R_Date("C9, 460+/-30", 460, 30);
  R_Date("C11, 105+/-35", 105, 35);
 };
 C_Date("Historical constraint", 1850 AD, 0);
 Difference("P5-P4 recurrence interval", "P5", "P4");
 Difference("P4-P3 recurrence interval", "P4", "P3");
 Difference("P3-P2 recurrence interval", "P3", "P2");
 Difference("P2-P1 recurrence interval", "P2", "P1");
 Boundary("end");
};
```

APPENDIX E

SLIP-RATE ESTIMATES FOR THE RICE CREEK SITE

Displacement (m)[1]

Earthquake	min	max
1	1.3	2.7
2	2.7	3.7
3	0.8	1.4
4	1.6	2.3
5	1.6	2.3
6	0.6	0.7
Mean (excluding earthquake 6)	**1.6**	**2.5**

Earthquake recurrence (yr)[2]

Earthquakes	min	max
1-2	190	810
2-3	620	2710
3-4	380	3270
4-5	320	3300
5-6	280	4430
Mean (earthquakes 5-2):	**440**	**3093**

Interval slip rates (mm/yr)[3]

Earthquakes	min	max
1-2	1.6	14.2
2-3	1.0	6.0
3-4	0.2	3.7
4-5	0.5	7.2
5-6	0.4	8.2
Mean:	**0.7**	**7.9**

Net displacement/offset (m)[4]

Method	min	max
Projection	8.0	12.4
Graphical reconstruction	9.5	9.9
Scarp-profile net offset	9.3	11.5

Elapsed time (kyr)[5]

	min	max
Elapsed time between earthquake 6 and 1		
Earthquake 6 (ka)	7.8	9.9
Earthquake 1 (ka)	0.5	0.6
Elapsed time (kyr)	7.2	9.4
Fan age minus elapsed time from earthquake 1 to present		
L1 and L6 minus P1 (kyr)	4.2	9.4

Site slip rates (mm/yr)[6]

	min	max
	0.8	1.7
	1.0	1.4
	1.0	1.6
Mean:	**0.9**	**1.6**
	0.9	3.0
	1.0	2.4
	1.0	2.8
Mean:	**0.9**	**2.7**
Mean (site):	**0.9**	**2.1**

[1] Displacement per event; see text for discussion. Mean displacement is range from mean of minimum values to mean of maximum values, excluding the poorly defined earthquake 6 displacement estimate.

[2] Earthquake-recurrence intervals are two-sigma ranges based on OxCal model D. Mean estimate is based on the three intervals between earthquakes 5 and 2.

[3] Interval slip rates are determined by dividing the per-event vertical displacements (e.g., 1.3-2.7 m for earthquake 1) by the previous recurrence intervals (e.g., 190-810 yr between earthquakes 2 and 1).

[4] Total site displacement, based on the projections of stratigraphic contacts and geomorphic surfaces (plate 2), our graphical reconstruction of faulting (plate 2), and the net site offset based on our scarp-profile data (figure 6). These estimates do not account for displacement in earthquake 6.

[5] Elapsed time between earthquakes and the approximate age of the Rice Creek alluvial fan, based on two-sigma earthquake times and luminescence ages.

[6] Average slip rates for the Rice Creek site. Minimum and maximum values are the minimum and maximum net displacements divided by the upper- and lower-bound elapsed time intervals. Mean slip rate for the site ranges from mean of all minimum values to mean of all maximum values.

EXPLANATION

- s4 — A horizon of soil developed on underlying unit (e.g., soil on unit 4 [s4])
- Infilled burrow
- Block in colluvial unit
- Unit description location; labelled where multiple descriptions per unit
- Bulk-soil sample for radiocarbon analysis
- Sample for luminescence dating
- OG — Open-work gravel lens
- Gravel and boulders
- Contact; well located, dashed where indistinct
- Contact between wash (e.g., 1a) and debris (e.g., 1b) facies of scarp-derived colluvium
- Intra-unit bedding
- Base of A horizon
- Fracture
- Fault; arrows indicate direction of relative movement; dashed where indistinct and numbered sequentially from east to west
- Eroded fault-scarp free face; dashed were indistinct

Footwall of upper fault zone

- 4c, 4c-1, 4c-2, 4c-3 — Stream and debris-flow deposits

Hanging wall of upper fault zone
Footwall of lower fault zone

- 1b, 1a — Scarp colluvium (earthquake U1) (1a) debris facies (1b) wash facies
- 2, 2b, 2a — Scarp colluvium (earthquake U2) (1a) debris facies (1b) wash facies
- 3, 3b, 3a — Scarp colluvium (earthquake U3) (1a) debris facies (1b) wash facies
- 4s — Sheared sediment
- 4b: 4b-df — Debris-flow deposit
- 4b: 4b-sd — Stream deposit
- 4b: 4b-1, 4b-2, 4b-3 — Stream and debris-flow deposits
- 5 — Scarp colluvium (earthquake L4)
- 6-1, 6-2 — Stream and debris-flow deposits

Hanging wall of lower fault zone

- 1, 1b, 1a — Scarp colluvium (earthquake L1) (1a) debris facies (1b) wash facies
- 2, 2b, 2a — Scarp colluvium (earthquake L2) (1a) debris facies (1b) wash facies
- 3 — Mixed scarp colluvium (earthquake L3) and alluvium
- 4s — Sheared sediment
- 4a: 4a-1 — Stream and debris-flow deposits
- 4a: 4a-df — Debris-flow deposit
- 4a: 4a-2, 4a-3 — Stream and debris-flow deposits including subunits 4a-3a and 4a-3b (stream deposits)
- 4a: 4a-sd — Stream deposit
- 4a: 4a-4 — Stream deposit

Antithetic fault zone

- 1b, 1a — Scarp colluvium (earthquake AL1) (1a) debris facies (1b) wash facies
- 2 — Scarp colluvium (earthquake AL2)

South trench wall

- 3a-1, 3a-2, 3a-3 — Stream and debris-flow deposits

North trench wall

- 3b-1, 3b-2, 3b-3 — Stream and debris-flow deposits

NOTES

Stratigraphic units and soils are described in appendix A.

Bulk-soil samples (e.g., C1) and radiocarbon ages (e.g., 2340-2680 cal yr B.P.) are summarized in appendix B.

Optically stimulated luminescence samples (e.g., L1) and ages (e.g., 4.8-9.0 ka) are summarized in appendix C.

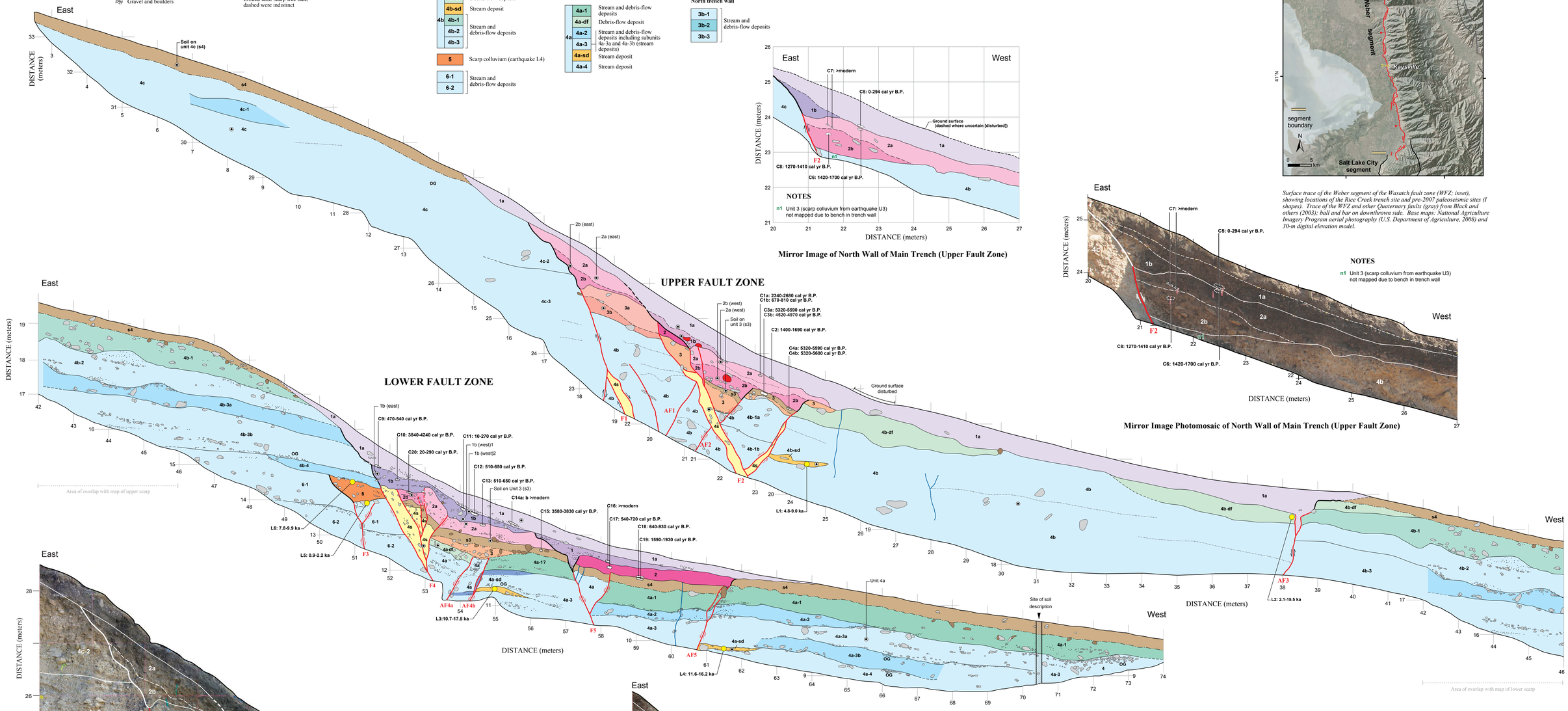

Mirror Image of North Wall of Main Trench (Upper Fault Zone)

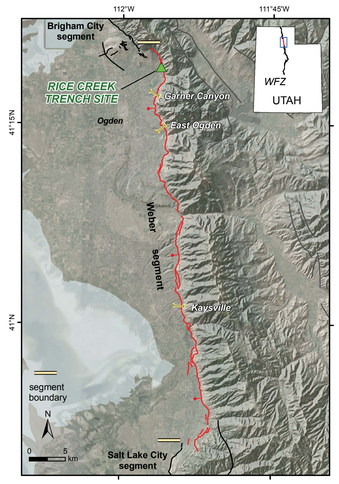

Surface trace of the Weber segment of the Wasatch fault zone (WFZ; inset), showing locations of the Rice Creek trench site and pre-2007 paleoseismic sites (1 shapes). Trace of the WFZ and other Quaternary faults (gray) from Black and others (2003); ball and bar on downthrown side. Base maps: National Agriculture Imagery Program aerial photography (U.S. Department of Agriculture, 2008) and 30-m digital elevation model.

Mirror Image Photomosaic of North Wall of Main Trench (Upper Fault Zone)

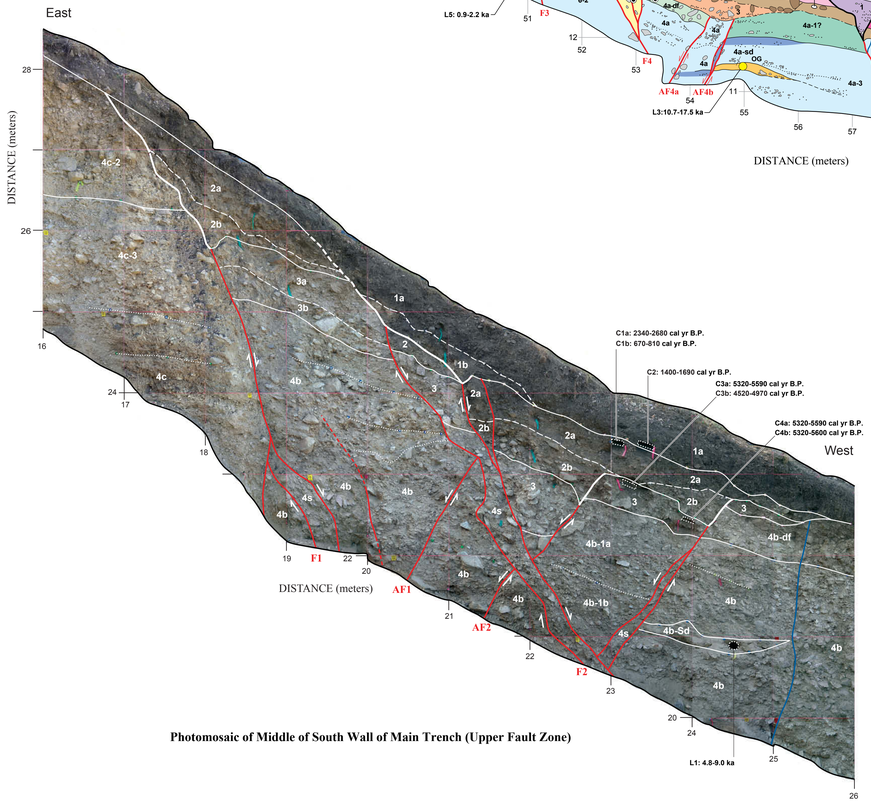

Photomosaic of Middle of South Wall of Main Trench (Upper Fault Zone)

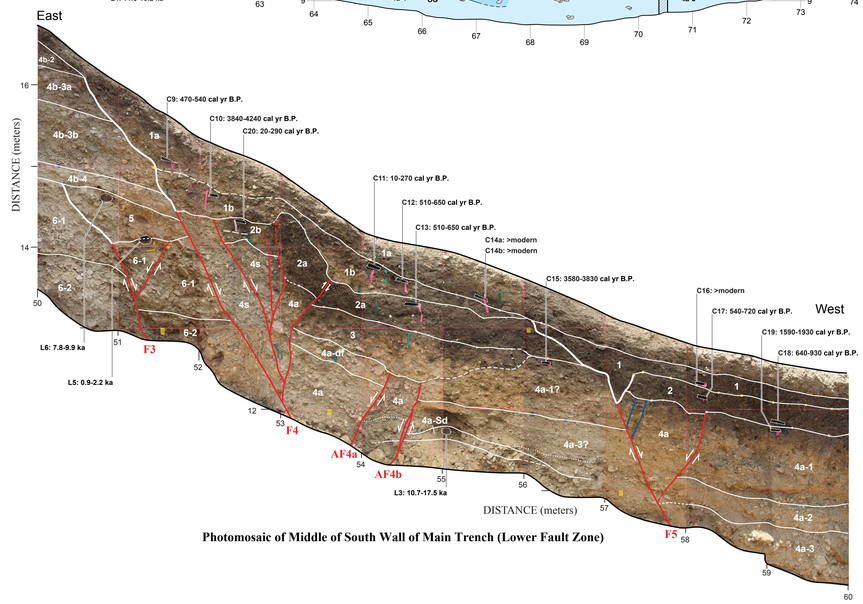

Photomosaic of Middle of South Wall of Main Trench (Lower Fault Zone)

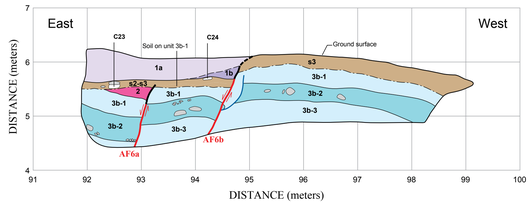

Mirror Image of North Wall of Antithetic Trench

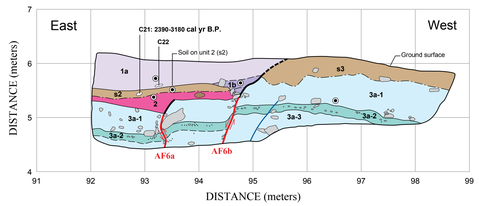

South Wall of Antithetic Trench

Although this product represents the work of professional scientists, the Utah Department of Natural Resources, Utah Geological Survey, makes no warranty, expressed or implied, regarding its suitability for a particular use. The Utah Department of Natural Resources, Utah Geological Survey, shall not be liable under any circumstances for any direct, indirect, special, incidental, or consequential damages with respect to claims by users of this product.

STRATIGRAPHIC AND STRUCTURAL RELATIONS AT THE RICE CREEK TRENCH SITE, WEBER SEGMENT, WASATCH FAULT ZONE

by Christopher B. DuRoss, Stephen F. Personius, Anthony J. Crone, Greg N. McDonald, and David J. Lidke

UPPER FAULT ZONE RECONSTRUCTION

Alluvial-Fan Deposition

Intermittent alluvial-fan deposition from before 7.8-9.9 ka (luminescence sample L6; appendix C) until shortly after 4.8-9.0 ka (L1)

Earthquake U3

A: 2.5 m of vertical displacement on fault F1

B: 0.5 m of antithetic-fault displacement on fault AF3

C: Near-fault rotation (10 degrees counterclockwise) of antithetic-fault AF3 footwall

D: Deposition of U3 scarp colluvium

E: Initial A-horizon development on alluvial-fan surface and U3 colluvium

Earthquake U2

A: 2.5 m of vertical displacement on fault F1

B: 0.5 m antithetic-fault displacement on fault AF3

C: Blocks of alluvial-fan deposits on hanging wall of fault F1 displaced down-to-the-east and rotated 3-5 degrees clockwise on faults AF1 and AF2

D: Deposition of earthquake U2 scarp colluvium

E: A-horizon development on alluvial-fan surface and U2 colluvium

Earthquake U1

A: 1.6 m of vertical displacement on fault F2

B: Deposition of earthquake U1 scarp colluvium

C: A-horizon development on alluvial-fan surface and U1 colluvium (not mapped)

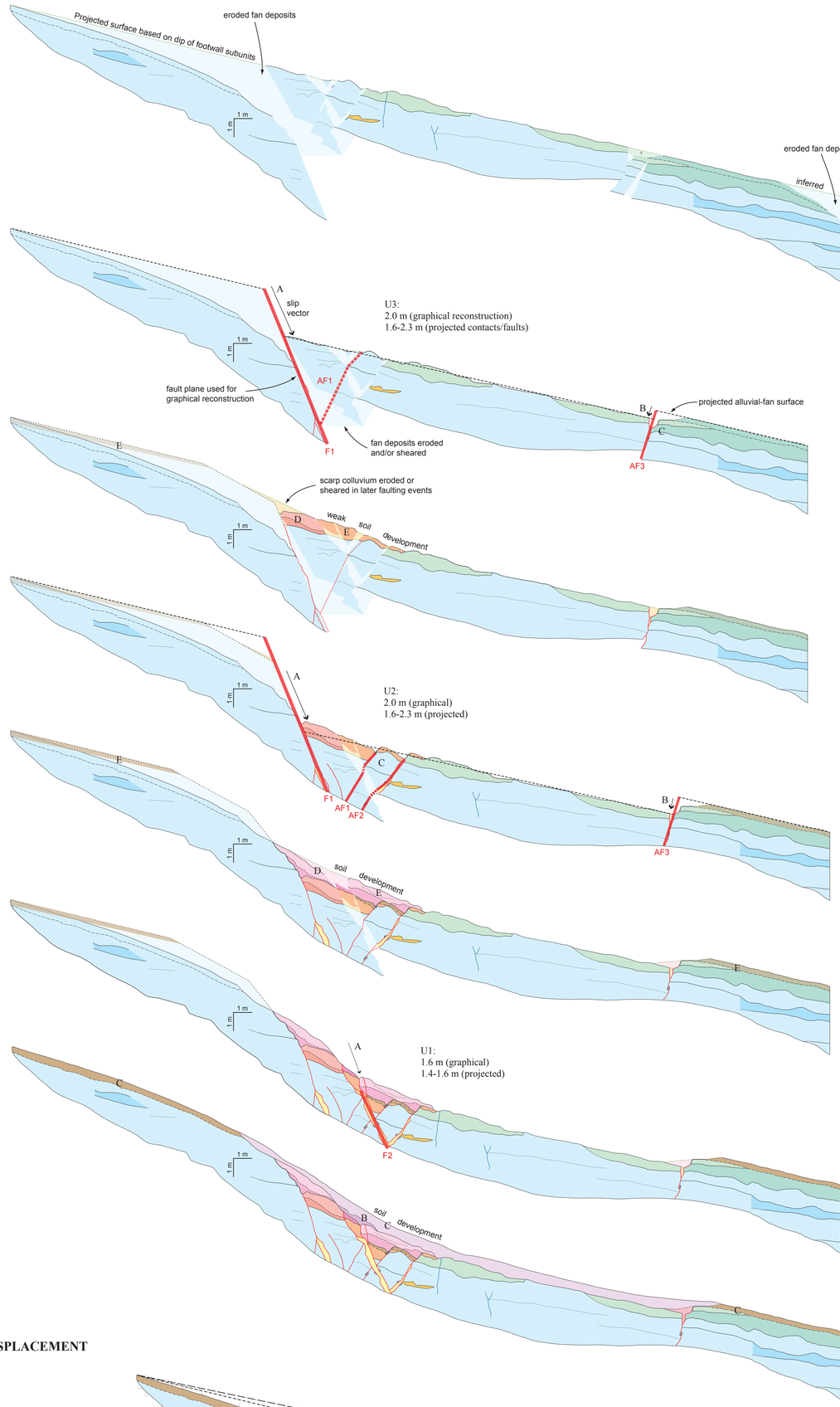

LOWER FAULT ZONE RECONSTRUCTION

Earthquakes L4 and L3

A: Earthquake L4. Minimum of 0.6 m of vertical displacement on fault F3 (not restored)

B: Earthquake L3. 0.8 m of antithetic-fault displacement on fault AF4 (not restored)

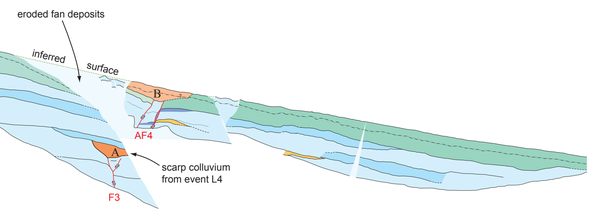

Earthquake L2

A: 2 m of vertical displacement on fault F4

B: 0.5 m antithetic-fault displacement on fault AF5

C: Near-fault drag (6.5 degrees counterclockwise) in footwall of antithetic fault AF5

D: Deposition of earthquake L2 scarp colluvium

E: A-horizon development on alluvial-fan surface and L2 colluvium (not mapped)

Earthquake L1

A: 2 m vertical displacement on fault F4

B: Blocks of alluvial-fan deposits and L2 colluvium compressed along fault F4

C: 0.6 m synthetic displacement on fault F5 (about one-half accommodated by 3 degrees of counterclockwise hanging-wall rotation)

D: 1-m-wide block bounded by minor fault antithetic to fault F5 rotates 7 degrees clockwise

E: Deposition of earthquake L1 scarp colluvium

F: A-horizon development on alluvial-fan surface and L1 colluvium (not mapped)

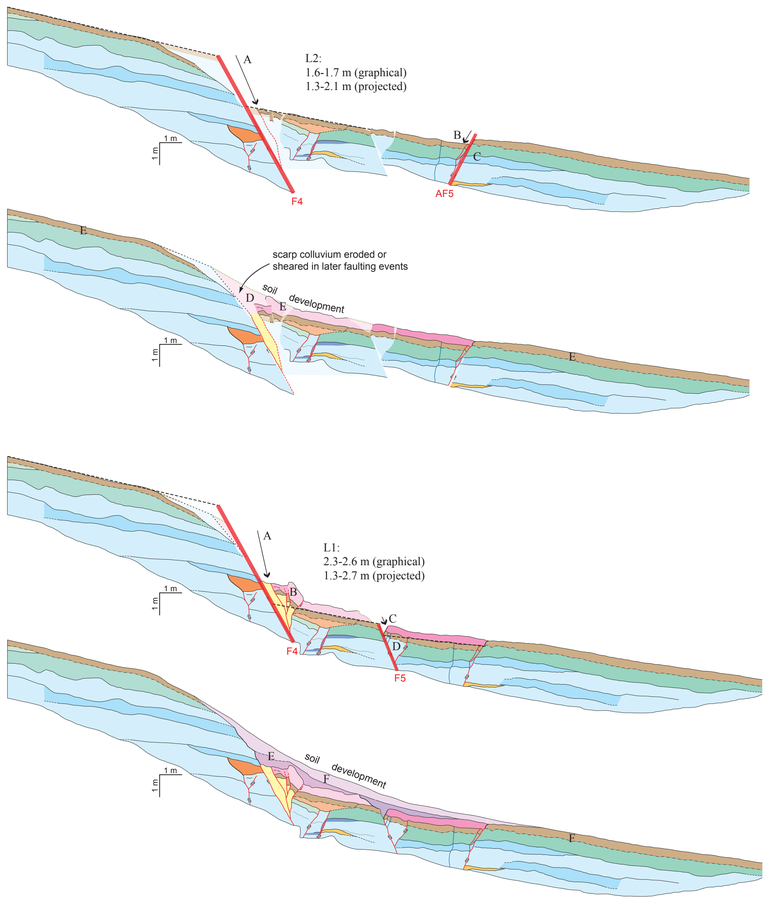

SUMMARY OF VERTICAL DISPLACEMENTS

Graphical Reconstruction	Projection Method
U3: 2.0 m	U3: 1.6-2.3 m
U2: 2.0 m	U2: 1.6-2.3 m
U1: 1.6 m	U1: 1.4-1.6 m
L4: NA	L4: >0.6-0.7 m
L3: NA	L3: 0.8-1.4 m
L2: 1.6-1.7 m	L2: 1.3-2.1 m
L1: 2.3-2.6 m	L1: 1.3-2.7 m

Sum of Graphical Reconstruction

9.5-9.9 m

Sum of Projection-Based Displacement

8.0-12.4 m (excluding L4 displacement)

Scarp-Profile Vertical Offset

9.3-11.5 m (includes antithetic fault zone; figure 6)

PROJECTION-BASED DISPLACEMENT

Earthquakes U3 and U2

A: Net displacement: 4.8-5.3 m,
from projections of (1) the uppermost alluvial-fan surface based on the dip of subunits in the footwall of fault F1, (2) the uppermost alluvial-fan surface based on the scarp profile, and (3) the alluvial-fan surface in the hanging wall of fault F1, outside of the upper fault zone (west of fault AF3; using surface-slope projection)

Displacement per events U3 and U2: 3.2-4.0 m (1.6-2.0 m per event), based on net displacement (4.8-5.3 m), minus U1 displacement (1.4-1.6 m), divided by two

B: Net displacement 5.4-5.9 m,
from projections of (1) the uppermost alluvial-fan surface based on the dip of subunits in the footwall of fault F1, (2) the uppermost alluvial-fan surface based on the scarp profile, and (3) the alluvial-fan surface in the hanging wall of fault F1, outside of the upper fault zone (west of fault AF3; using the dip of fan subunits)

Displacement per events U3 and U2: 3.8-4.6 m (1.9-2.3 m per event), based on net displacement (5.4-5.9 m), minus U1 displacement (1.4-1.6 m), minus antithetic displacement (0.5 m), divided by two

C: Net displacement 6.0-6.5 m,
from projections of (1) the uppermost alluvial-fan surface based on the dip of subunits in the footwall of fault F1, (2) the uppermost alluvial-fan surface based on the scarp profile, and (3) the alluvial-fan surface in the hanging wall of fault F1, west of the fault zone (between faults F2 and AF3)

Displacement per events U3 and U2: 4.0-4.6 m (2.0-2.3 m per event), based on net displacement (6.0-6.5 m), minus U1 displacement (1.4-1.6 m), minus antithetic displacement (0.5 m), divided by two

Earthquake U1

D: 1.5-1.6 m based on the base of scarp colluvium from earthquake U2

E: 1.4-1.5 m based on faults AF1 and AF2 formed in earthquake U2 and displaced in U1

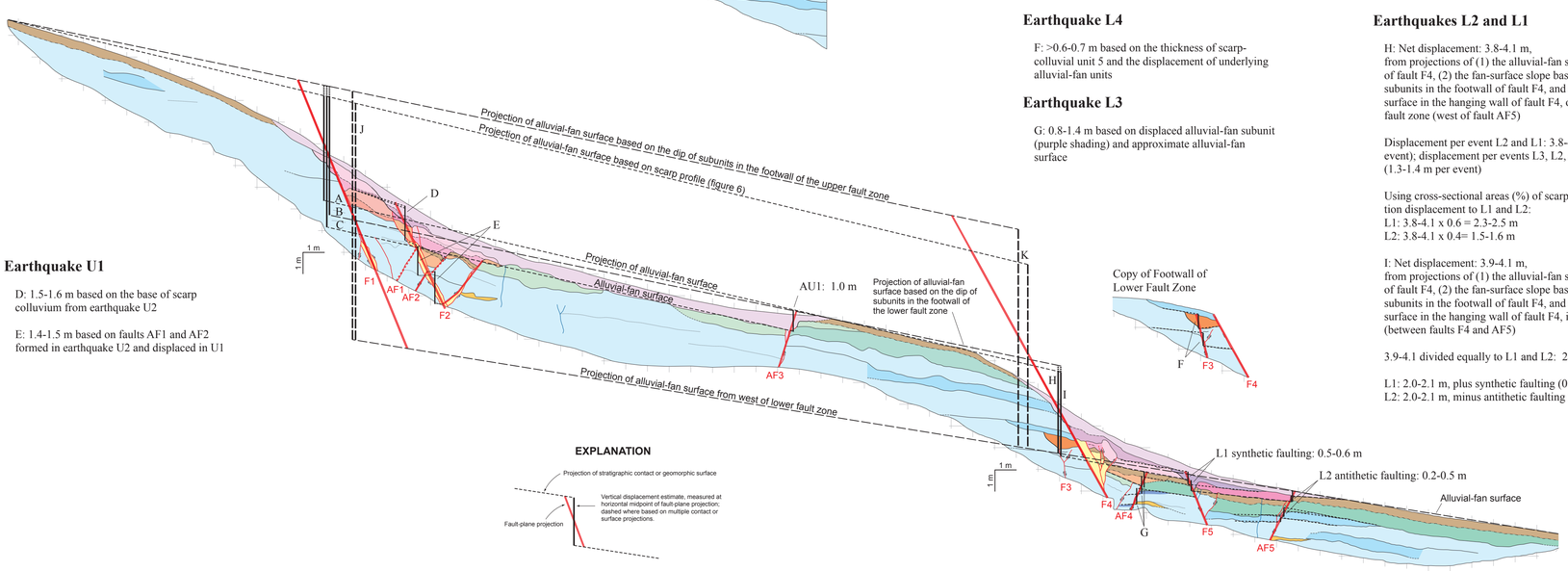

Earthquake L4

F: >0.6-0.7 m based on the thickness of scarp-colluvial unit 5 and the displacement of underlying alluvial-fan units

Earthquake L3

G: 0.8-1.4 m based on displaced alluvial-fan subunit (purple shading) and approximate alluvial-fan surface

Earthquakes L2 and L1

H: Net displacement: 3.8-4.1 m,
from projections of (1) the alluvial-fan surface in the footwall of fault F4, (2) the fan-surface slope based on the dip of subunits in the footwall of fault F4, and (3) the alluvial-fan surface in the hanging wall of fault F4, outside of the main fault zone (west of fault AF5)

Displacement per event L2 and L1: 3.8-4.1 m (1.9-2.1 m per event); displacement per events L3, L2, and L1: 3.8-4.1 m (1.3-1.4 m per event)

Using cross-sectional areas (%) of scarp colluvium to apportion displacement to L1 and L2:
L1: 3.8-4.1 x 0.6 = 2.3-2.5 m
L2: 3.8-4.1 x 0.4= 1.5-1.6 m

I: Net displacement: 3.9-4.1 m,
from projections of (1) the alluvial-fan surface in the footwall of fault F4, (2) the fan-surface slope based on the dip of subunits in the footwall of fault F4, and (3) the alluvial-fan surface in the hanging wall of fault F4, in the main fault zone (between faults F4 and AF5)

3.9-4.1 divided equally to L1 and L2: 2.0-2.1 m per event

L1: 2.0-2.1 m, plus synthetic faulting (0.5-0.6 m): 2.5-2.7m
L2: 2.0-2.1 m, minus antithetic faulting (0.2-0.5 m): 1.5-1.9 m

Net Site Displacement

J: 10.9-11.4 m based on the projection of alluvial-fan surfaces toward the upper fault zone

K: 8.5-9.0 m based on the projection of alluvial-fan surfaces toward the lower fault zone

Although this product represents the work of professional scientists, the Utah Department of Natural Resources, Utah Geological Survey, makes no warranty, expressed or implied, regarding its suitability for a particular use. The Utah Department of Natural Resources, Utah Geological Survey, shall not be liable under any circumstances for any direct, indirect, special, incidental, or consequential damages with respect to claims by users of this product.

STRUCTURAL RESTORATION OF THE MAIN TRENCH, RICE CREEK TRENCH SITE, WEBER SEGMENT, WASATCH FAULT ZONE

by Christopher B. DuRoss, Stephen F. Personius, Anthony J. Crone, Greg N. McDonald, and David J. Lidke